

University of Windsor

## Scholarship at UWindor

---

Electronic Theses and Dissertations

Theses, Dissertations, and Major Papers

---

2012

### Development of an Ultrasonic Linear Phased Array System for Real-time Quality Monitoring of Resistance Spot Welds

Anthony Lui  
*University of Windsor*

Follow this and additional works at: <https://scholar.uwindsor.ca/etd>

---

#### Recommended Citation

Lui, Anthony, "Development of an Ultrasonic Linear Phased Array System for Real-time Quality Monitoring of Resistance Spot Welds" (2012). *Electronic Theses and Dissertations*. 4826.  
<https://scholar.uwindsor.ca/etd/4826>

This online database contains the full-text of PhD dissertations and Masters' theses of University of Windsor students from 1954 forward. These documents are made available for personal study and research purposes only, in accordance with the Canadian Copyright Act and the Creative Commons license—CC BY-NC-ND (Attribution, Non-Commercial, No Derivative Works). Under this license, works must always be attributed to the copyright holder (original author), cannot be used for any commercial purposes, and may not be altered. Any other use would require the permission of the copyright holder. Students may inquire about withdrawing their dissertation and/or thesis from this database. For additional inquiries, please contact the repository administrator via email ([scholarship@uwindsor.ca](mailto:scholarship@uwindsor.ca)) or by telephone at 519-253-3000ext. 3208.

Development of an Ultrasonic Linear Phased Array System for Real-time Quality  
Monitoring of Resistance Spot Welds

by

Anthony Lui

A Thesis

Submitted to the Faculty of Graduate Studies  
through Electrical and Computer Engineering  
in Partial Fulfillment of the Requirements for  
the Degree of Master of Applied Science at the  
University of Windsor

Windsor, Ontario, Canada

2012

© 2012 Anthony Lui

Development of an Ultrasonic Linear Phased Array System for Real-time Quality  
Monitoring of Resistance Spot Welds

by

Anthony Lui

APPROVED BY:

---

Dr. Wladyslaw Kedzierski  
Department of Physics

---

Dr. Maher Sid-Ahmed  
Department of Electrical and Computer Engineering

---

Dr. Roman Maev, Principal Advisor  
Department of Electrical and Computer Engineering / Physics

---

Dr. Esam Abdel-Raheem, Chair of Defense  
Department of Electrical and Computer Engineering

August 22, 2012

## DECLARATION OF CO-AUTHORSHIP

I hereby declare that this thesis incorporates material that is result of joint research as follows:

This thesis also incorporates the results of a joint research undertaken in collaboration between the University of Windsor and the University of Florence under the supervision of Dr. Roman Maev. The collaboration is covered in Chapter 3.3. of the thesis. In all cases, the key ideas, primary contributions, experimental designs, data analysis and interpretations, were performed by the author with support from supervisors.

I am aware of the University of Windsor Senate Policy on Authorship and I certify that I have properly acknowledged the contribution of other researchers to my thesis, and have obtained written permission from each of the co-author(s) to include the above material(s) in my thesis.

I certify that, with the above qualification, this thesis, and the research to which it refers, is the product of my own work.

I declare that, to the best of my knowledge, my thesis does not infringe upon anyone's copyright nor violate any proprietary rights and that any ideas, techniques, quotations, or any other material from the work of other people included in my thesis, published or otherwise, are fully acknowledged in accordance with the standard referencing practices. Furthermore, to the extent that I have included copyrighted material that surpasses the bounds of fair dealing within the meaning of the Canada Copyright Act, I certify that I have obtained a written permission from the copyright owner(s) to include such material(s) in my thesis and have included copies of such copyright clearances to my appendix.

I declare that this is a true copy of my thesis, including any final revisions, as approved by my thesis committee and the Graduate Studies office, and that this thesis has not been submitted for a higher degree to any other University or Institution.

## ABSTRACT

This thesis presents research in the development of using an ultrasonic linear phased array transducer for real-time quality monitoring of resistance spot welds. Existing in-line systems use a single element transducer installed inside the welding electrode which capture the entire welding process. The single element system can very accurately determine the quality of a spot weld by acquiring A-scans through the center of the heat affected zone during welding. The linear phased array system being presented extends on the existing single element system utilizing a 24 element linear array transducer. By having 24 elements, the setup presented has the capability to inspect an entire line through the heat affected zone. This system makes it possible to measure the nugget diameter and detect potential voids inside the weld nugget, thus potentially improving in-line, non-destructive evaluation of spot welds.

## DEDICATION

This thesis is dedicated to my loving parents, sister, and girlfriend for all their support and encouragement.

## ACKNOWLEDGEMENTS

I would like to acknowledge many people who have supported me and helped me overcome the many challenges I have faced while completing my Master's Degree. I sincerely thank my supervisor, Dr. Roman Maev who gave me the wonderful opportunity to join his research team and provided me with invaluable advice, guidance and support to help me succeed.

My committee members Dr. Kedzierski and Dr. Sid-Ahmed gave constructive evaluation and suggestions in my seminar and in the review of this thesis to ensure it met their requirements.

I am glad to have had the opportunity to work with the members of Dr. Meav's research group. It was a great pleasure working with the In-line team, Dr. Andrew Chertov, Anthony Karloff, and Waldo Perez. Many thanks to Dmitry Gavrilov, Kiyanoosh Shapoori, and Dr. Jeff Saddler. Also, thanks to Sarah Beneteau, Sabina Baraoniciu, and Suong Mancini for always being available in the office for assistance.

I am grateful for the assistance provided by Dr. Piero Tortoli, Dr. Alessandro Dallai, and Dr. Enrico Boni from the University of Florence. The ULA-OP system they developed was a key tool used in my research.

I am indebted to my parents for always being supportive and giving me the confidence to take on any challenges in life. My sister Kirsten, was always there whenever I needed her. My girlfriend Minh was always understanding of my busy schedule. I feel blessed to have so much love and support around me.



## TABLE OF CONTENTS

DECLARATION OF CO-AUTHORSHIP .....	iii
ABSTRACT .....	v
DEDICATION .....	vi
ACKNOWLEDGEMENTS .....	vii
LIST OF TABLES .....	x
LIST OF FIGURES .....	xi
<b>CHAPTER 1</b>	
<b>INTRODUCTION</b>	
1.1. Overview .....	1
1.2. Thesis Outline .....	3
<b>CHAPTER 2</b>	
<b>BACKGROUND &amp; RELATED WORK</b>	
2.1. Resistance Spot Welding.....	5
2.2. Off-line Destructive Testing of Resistance Spot Welds .....	7
2.3. Off-line Ultrasonic Non-Destructive Evaluation Methods .....	8
2.4. Existing Single Element In-line System .....	9
2.5. Phased Arrays & Beam-steering .....	12
<b>CHAPTER 3</b>	
<b>DESIGN AND METHODOLOGY</b>	
3.1. Focusing Through Different Media & Snell's Law .....	14
3.2. Transducer Design .....	17
3.3. ULA-OP Device.....	20
3.4. Transducer Housing Design.....	24
<b>CHAPTER 4</b>	
<b>ANALYSIS OF RESULTS</b>	
4.1. Preliminary Results .....	28
4.2. Off-line Spot Weld Evaluation Using Existing Methods.....	37
4.3. Real-time Spot Weld Monitoring.....	44

## **CHAPTER 5**

### **CONCLUSIONS AND RECOMMENDATIONS**

5.1. Conclusions .....	53
5.2. Recommendations .....	55

<b>REFERENCES.....</b>	<b>57</b>
------------------------	-----------

### **APPENDICES**

ULA-OP Files & Code .....	59
A.1. Calculating Transmission and Reception Delays .....	59
A.2. Generating bft Files for Transmission .....	65
A.3. Generating bfr Files for Reception .....	65
A.4. ULA-OP Configuration File (.cfg) .....	66
A.5. ULA-OP ULA File (.ula).....	68
Image Processing MATLAB Code.....	69
B.1. Slot Size Measurement.....	69
B.2. Weld Nugget Size Measurement.....	72

<b>VITA AUCTORIS .....</b>	<b>77</b>
----------------------------	-----------

## LIST OF TABLES

TABLE 3.2.1. LINEAR PHASED ARRAY SPECIFICATIONS. ....	20
TABLE 3.3.1. ULA-OP MAIN FEATURES.....	22
TABLE 4.1.1. CALCULATED SLOT SIZES.....	37
TABLE 4.2.1. ACOUSTIC MICROSCOPE C-SCANS (10 MM X 10 MM) OF WELDS WITH MEASUREMENTS. ....	41
TABLE 4.2.2. CROSS-SECTIONS OF WELDS.....	43
TABLE 4.2.3. PEEL TEST NUGGET DIAMETERS. ....	44
TABLE 4.3.1. CALCULATED NUGGET DIAMETERS. ....	52

## LIST OF FIGURES

FIGURE 2.1.1. RESISTANCE SPOT WELDING STAGES.....	6
FIGURE 2.4.1. SINGLE ELEMENT TRANSDUCER INSTALLED IN WATER STREAM.....	10
FIGURE 2.4.2. A-SCANS ACQUIRED WITH NO NUGGET (TOP) AND NUGGET PRESENT (BOTTOM). ....	10
FIGURE 2.4.3. M-SCAN WITH KEY FEATURES HIGHLIGHTED. ....	11
FIGURE 2.5.1. BEAM-STEERING EXAMPLE. ....	13
FIGURE 3.1.1. SNELL’S LAW WITH $v_2 < v_1$ .....	14
FIGURE 3.1.2. SPOT WELDING MEDIA (WATER, COPPER, STEEL). ....	15
FIGURE 3.1.3. RECEPTION LINES WITH REFRACTION IN WELDING SETUP. ....	16
FIGURE 3.2.1. SCHEMATIC OF GENERIC PHASED ARRAY. ....	18
FIGURE 3.3.1. ULA-OP OVERVIEW.....	21
FIGURE 3.3.2. ULA-OP MODULE – REAL-TIME SOFTWARE.....	22
FIGURE 3.4.1. INITIAL TRANSDUCER HOUSING DESIGN.....	25
FIGURE 3.4.2. FINAL TRANSDUCER HOUSING DESIGN. ....	26
FIGURE 3.4.3. MANUFACTURED BENT ADAPTER (LEFT) AND ASSEMBLED HOUSING (MIDDLE & RIGHT).....	26
FIGURE 3.4.4. FINAL ASSEMBLY.....	27
FIGURE 4.1.1. PLATES WITH HOLES (TOP) & SLOTS (BOTTOM). ....	28
FIGURE 4.1.2. SYNTHETIC B-SCAN OF A 2 MM HOLE / SLOT.....	29
FIGURE 4.1.3. B-SCANS OF HOLES (1.5 MM TO 7 MM). ....	30
FIGURE 4.1.4. B-SCANS OF SLOTS (1.5 MM TO 7 MM). ....	31
FIGURE 4.1.5. FREQUENCY RESPONSE OF FINITE IMPULSE RESPONSE (FIR) FILTER.....	33

FIGURE 4.1.6. B-SCANS W/ RADIO FREQUENCY DATA (LEFT) & DEMODULATED DATA (RIGHT). .....	33
FIGURE 4.1.7. INTERPOLATED B-SCAN WITH WINDOW (LEFT) & AMPLITUDE PLOT (RIGHT). .....	34
FIGURE 4.1.8. GAUSSIAN CURVE. ....	35
FIGURE 4.1.9. AMPLITUDE PLOT WITH GAUSSIAN FIT. ....	35
FIGURE 4.1.10. GAUSSIAN FIT ON SEVERAL SLOT SIZES. ....	36
FIGURE 4.3.1. SCHEMATIC OF WELD GEOMETRY (TOP) VS. ACQUIRED B-SCAN (BOTTOM)..	45
FIGURE 4.3.2. B-SCANS OF SEVERAL SPOT WELDING STAGES. ....	46
FIGURE 4.3.3. WELD 10kA-A B-SCAN (LEFT) WITH CROSS-SECTION (RIGHT).....	47
FIGURE 4.3.4. SINGLE ELEMENT M-SCAN (LEFT) AND LINEAR PHASED ARRAY M-SCAN (RIGHT). .....	48
FIGURE 4.3.5. ORIGINAL M-SCAN (LEFT) &. DERIVATIVE ENHANCED M-SCAN (RIGHT).....	49
FIGURE 4.3.6. DERIVATIVE ENHANCED M-SCAN (LEFT) & FILTER ENHANCED M-SCAN (RIGHT). .....	50
FIGURE 4.3.7. M-SCAN WITH HIGHLIGHTED LINE. ....	51

# CHAPTER 1

## INTRODUCTION

### 1.1. Overview

The research being presented extends on existing in-line single element transducer systems for real time quality evaluation of resistance spot welds. It begins investigating the feasibility of ultrasonic phased arrays in spot welding applications. Ideally, a two-dimensional phased array could monitor an entire spot weld over the welding process. A two-dimensional phased array however, could be quite costly to manufacture. A linear phased array is a more economical solution but has the disadvantage of only being able to monitor a cross-section through a spot weld over the welding process. Both two-dimensional phased arrays and linear phased arrays follow the same principles in their operation, so using a linear phased array is an economic proof of concept before extending to a two-dimensional phased array. As with many electronics, as technology advances, the cost to manufacture electronics decreases. Two-dimensional phased arrays could be costly now but it is fairly safe to assume that the cost to manufacture them will decrease as technology advances.

By using an ultrasonic linear phased array, acoustic energy can be focused through beam-steering techniques such that an entire line through a spot weld can be monitored whereas only a single point through the center of a spot weld can be monitored by existing single element systems. The images acquired by the linear phased array system in the welding process make it possible to measure nugget diameter and detect any voids inside the weld that are along the line being monitored.

The main objective of this research was to determine whether the existing in-line single element transducer system could be successfully extended to an in-line linear phased array system. Investigating the linear phased array system in spot welding is a proof of concept for a two-dimensional phased array system. In order to investigate the linear phased array, a device which can handle the transmission and reception for beam-steering was needed. In collaboration with the University of Florence, the ULA-OP device was used for controlling the transducer. The ULA-OP device is highly programmable and has the flexibility needed in this research application. The University of Florence provided support for the ULA-OP device in programming the device to work with the linear phased array. Very specific time delays needed to be calculated to be programmed into the ULA-OP device.

To attach the linear phased array to the weld gun, a transducer housing which could hold the transducer safely and be attached to the weld gun was needed. The housing had to also insulate the linear phased array transducer from electric current. The housing designs were reviewed by Centerline Limited and after some modifications, was manufactured. With the transducer housing along with the ULA-OP device, the spot welding process could be monitored in real-time. The acquisitions from the spot welding process were then analyzed and processed using various techniques to measure the nugget diameter.

Finished welds can be inspected in many ways to measure nugget diameter and to check for voids within the weld nugget. Cross-sections were done to view the completed weld in a view similar to the B-scans obtained. From a cross-section the nugget diameter in 1 direction and voids along one line through the weld can be viewed. Peel tests were

done to see and measure the actual nugget diameter obtained in both directions. Imaging with an acoustic microscope was also done to generate C-scans which provide an overhead view of the spot weld to measure nugget diameters and to detect any potential voids within the spot weld. The results and images acquired with the linear phased array system are compared to the alternative tests to verify their accuracy.

The quality of a spot weld in many cases, is extremely important. Many of these welds on a car body are crucial for safety. The linear phased array system makes it possible to observe a cross-section of a resistance spot weld in real-time while the weld is being performed. Ultimately, this research will predict how successfully the linear phased array system can be extended to a two-dimensional phased array system. A two-dimensional phased array system enable monitoring an entire weld in real-time. This will make it possible see the whole nugget profile and detect any voids present.

## 1.2. Thesis Outline

Chapter 2 covers some background and related work associated with resistance spot welding and ultrasonic transducers. An introduction to resistance spot welding is provided along with traditional off-line quality evaluation methods for spot welds. The existing single element in-line system for non-destructive evaluation of resistance spot welds is also covered in this chapter. An introduction to phased arrays and beam-steering is also provided.

Chapter 3 discusses the design and methodology behind the linear phased array system and setup. It covers beam-steering and focusing through the different media present in the spot welding setup. An overview of transducer design and the linear phased



array transducer used in the spot welding setup is provided. The ULA-OP device used to control the transducer and the housing used to hold the transducer is also presented.

Chapter 4 presents the results acquired from recording the welding process and the analysis of these results. Some preliminary results were gathered by imaging plates with holes and slots drilled into them. The spot welds which were recorded and monitored in the welding process were also evaluated using other offline methods such as acoustic imaging, cross-sections, and peel tests. The results from the offline methods of evaluation are also presented in this chapter and help verify what is actually being imaged by the linear phased array. An algorithm for measuring nugget diameters from the acquired M-scans is also presented

Chapter 5 discusses the conclusions reached from the study done on the ultrasonic linear phased array system for real-time quality monitoring of resistance spot welding. Recommendations and some improvements for future research in this field are also mentioned in this chapter.

## CHAPTER 2

### BACKGROUND & RELATED WORK

#### 2.1. Resistance Spot Welding

Welding is a process that joins materials such as metals or thermoplastics through the use of heat. Welding is a metallurgical process – all aspects of a welding process can be related to metallurgy of the materials involved in welding, either the base metal or the electrodes [1]. Resistance spot welding is one of the most commonly used methods for joining sheet metals. In the automotive industry many of the spot welds are crucial for the safety of a vehicle. Resistance spot welding uses joule heating to generate heat from electric current flow. Controlling the electrical and thermal parameters is common practice in resistance spot welding. The general expression of heat generated in an electric circuit is shown in Eqn. 2.1.1. where  $Q$  is heat,  $I$  is current,  $R$  is electrical resistance, and  $t$  is the time current flows in the circuit. In resistance welding, the heat generation at all locations in a weld region is more relevant than the total heat generated since heat should not be uniform in the weld region.

$$(Eqn. 2.1.1.) \quad Q = I^2 R t$$

The metal sheets are held together under very high pressure exerted by electrodes that were commonly made of a copper alloy [2]. There are two electrodes which are shaped to concentrate the welding current into a small spot as well as clamp the sheets together. By forcing a large amount of current through a fairly small spot, high amounts of heat are generated that melt the metal to form a weld. This entire process can occur in less than 300 ms without excessively heating the remainder of the sheet. There is also a cooling water stream inside the electrodes which keep the equipment from overheating

and only allow the heating and melting to occur between the metal sheets. The key stages in the resistance spot welding process are represented in Figure 2.1.1. From the initial stage, the welding electrodes are clamped together at a high pressure. Once the electrodes are clamped together and a good contact is made, the current is turned on which begins heating the interface between the two sheets. Current continues to flow as the interface begins to melt and to form a molten nugget between the two sheets. After a set duration, the molten nugget reaches a desirable size and current is turned off. Once the current is off the molten nugget begins to solidify, thus joining to the two metal sheets. Over the solidification period the electrodes remain closed in order to cool the material.

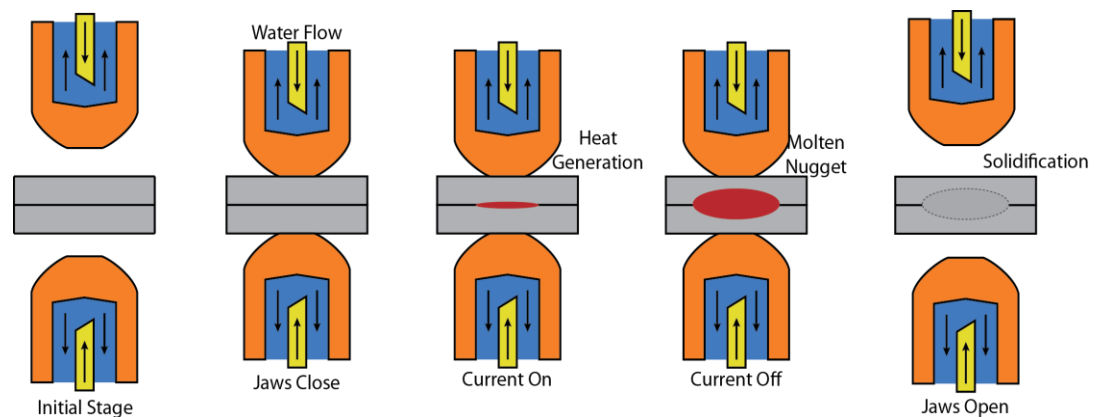


**Figure 2.1.1. Resistance spot welding stages.**

As represented from Eqn. 2.1.1, the amount of heat generated inside the welded region is determined by the resistance between the electrodes, the amount of current that is supplied and the duration in which the current is supplied. Selecting the correct amount of current is crucial to creating a good spot weld. Applying too little current won't melt the metal and will result in a poor weld. Applying too much current will melt too much metal and could cause ejection of molten material, called an expulsion. The diameter of the tip of the electrodes also determines the amount of current needed to produce a good weld. A larger diameter requires more current in order to maintain the same current

density. Thicker sheets also require more energy to be applied to the metal sheets. Resistance spot welding continues to be one of the most commonly used methods for joining sheet metals.

## 2.2. Off-line Destructive Testing of Resistance Spot Welds

There are several off-line methods used which inspect the quality of resistance spot welds. Destructive methods such as peel tests, chisel tests, and strength tests are commonly used methods. Destructive tests are usually done periodically but are costly and time consuming. In one case, the quality of the weld nuggets get checked after 15 cars are processed which occurs approximately once every two weeks [3]. The nuggets are examined off-line using destructive methods which take approximately 10 days to complete which causes a long delay in the production process. Jaguars' common industrial practice is to chisel test all welds on a single car every three months.

Peel tests as the name suggests, involve physically peeling a spot weld apart to reveal the weld nugget size and nugget diameter. Chisel tests can be both destructive and non-destructive. Chisel tests are performed by driving a chisel between spot welds or around spot welds until the material deforms. On bad or weak welds, the weld should break which would be considered a destructive test. Good welds also risk being damaged and having their strength reduced from the chisel tests. In some cases, after a weld has been chisel tested, the deformed metal can be hammered flat and the component could be used like normal which is considered a non-destructive test. Strength tests can also be performed by applying various stresses and strains to spot welds to reveal its strength against different forces [4]. This knowledge is important to determine whether a spot

weld is strong enough to withstand possible stresses and strains a weld could encounter in its application.

### 2.3.Off-line Ultrasonic Non-Destructive Evaluation Methods

Non-destructive evaluation is a broad field which involves testing components with an approach that will not affect the quality or performance of the component. The most commonly used off-line non-destructive evaluation methods today often involve the use of ultrasonic array transducers. Ultrasonic arrays are single transducers which contain a number of individually controlled elements. Ultrasonic arrays offer great potential to increase inspection quality and reduce inspection time [5]. The main advantage of using an array transducer is that one array can perform a number of different inspections on a component simultaneously and immediately create an image of the scanned area.

Ultrasonic array transducers are used both in medical imaging and in industry related applications. In the medical field, ultrasound can provide a non-invasive method for imaging various parts of the body including tendons, muscles, joints, vessels and internal organs. In industry, there are a wide variety of applications which can benefit from the use an array transducer. Some industrial applications of array transducers include, monitoring cracks inside steels blocks at high temperatures up to 400°C [6], testing nuclear power plant components [7], and inspection of components with complex geometry [8].

In resistance spot welding, an array transducer could be used to inspect and image the internal structure of the weld. This data could be used to determine the nugget size of the weld and detect any defects to help determine the quality of the weld. Periodic inspections of a welded car body could be a beneficial form of quality control without

needing to destruct the car body. There are even commercial devices which are specifically designed to analyze spot welds such as the Resistance Spot Weld Analyzer (RSWA) developed by Tessonics. Although off-line ultrasonic testing methods are quite reliable, the parts to be inspected must be removed from the production line and scanned manually. This procedure can be very time consuming, especially if every part needs to be inspected. In-line ultrasonic systems have been developed to inspect the quality of a resistance spot weld in real-time without needing to remove the part from the assembly line. This system is explained in more detail in section 2.4.

#### 2.4.Existing Single Element In-line System

Existing in-line single-element transducer systems have been successfully implemented in industry [9-10] for real-time evaluation of resistance spot welds. These systems primarily operate in pulse-echo mode. A piezoelectric transducer is installed inside the cooling water stream inside the welding electrode [11] as shown in Figure 2.4.1. The transducer transmits ultrasonic pulses every 3 ms and the reflections of the several interfaces are received by the same transducer and recorded as A-scans. Initially before any melting has occurred, reflections from the front wall, back wall, and the intermediate interface between the two metal plates are received. Once melting has occurred and a molten nugget has formed, the intermediate interface splits into two interfaces, one for the top of the liquid nugget and one for the bottom. A visual representation of this is shown in Figure 2.4.2. Successive A-scans are then combined to form an M-scan shown in Figure 2.4.3. which has key features on the M-scan highlighted. Each column of an M-scan represents a separate A-scan. On an M-scan the X and Y axes represent welding time and time of flight respectively. The entire welding

process is captured on the M-scan which carries valuable information for quality evaluation.

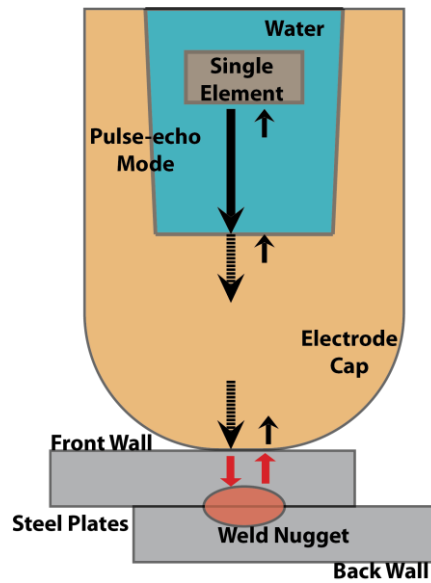


Figure 2.4.1. Single element transducer installed in water stream.

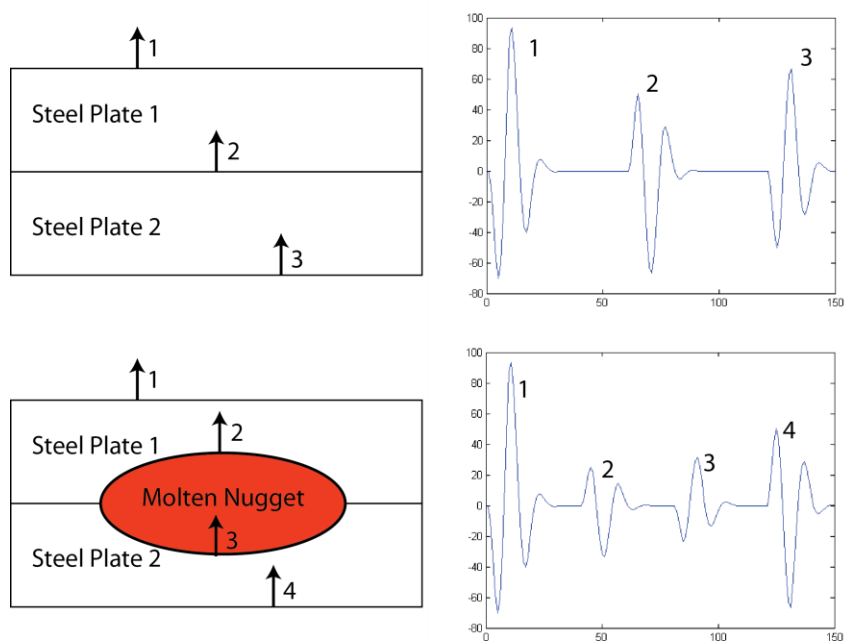
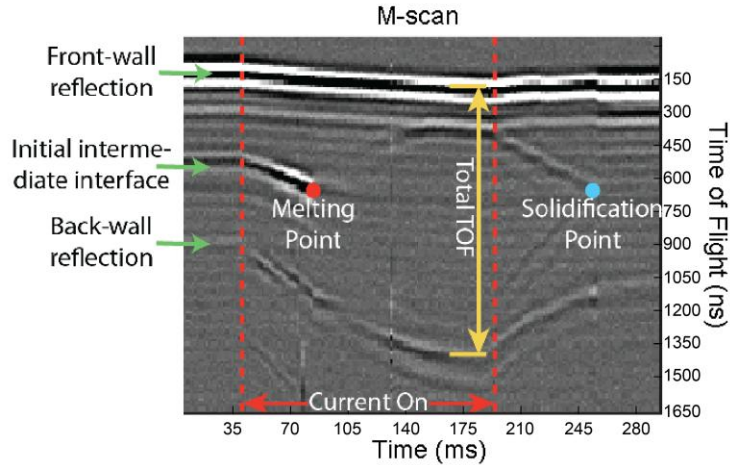


Figure 2.4.2. A-scans acquired with no nugget (top) and nugget present (bottom).



**Figure 2.4.3. M-scan with key features highlighted.**

From an M-scan, the exact moments in time when current is turned on or off and when melting or solidification occurs can be extracted. When melting occurs the intermediate interface on the M-scan disappears while the solid-liquid interfaces of the liquid nugget appear. Once the nugget solidifies, only the two front and back-wall reflections remain. An important parameter found on an M-scan is the total time of flight (TOF). This is the time required for the signal to travel from the front-wall to the back-wall and then back to the front-wall. Changes in TOF are observed whenever cooling or heating is occurring. As the temperature of a metal sample increase, the speed of sound decreases inside the sample, which increases the TOF between the front and back-wall. Using the M-scan acquired, this system also has the capabilities to detect expulsions and measure indentation [12], both of which can lower the weld strength and quality.

The in-line system performs automated analysis of M-scans in order to meet the requirements of the production environment. An advanced algorithm which performs multistage signal and image processing is used in order to automatically detect desired interfaces. These interfaces can be used to determine the quality of a weld and also



estimate the size of the liquid nugget. The ability to automatically inspect spot welds in real-time could help save time and money.

## 2.5. Phased Arrays & Beam-steering

Phased array transducers are multi-element transducers where each transducer can be controlled individually. By varying the timing of each element, the ultrasonic signal can be focused or steered. The main advantage of using a phased array transducer is the ability to electronically steer a beam without any mechanically moving components. This allows several areas to be inspected in a short amount of time. Figure 2.5.1. shows an example of beam-steering towards a target or focal point. The green bars represent the adjusted time delays for transmission. Elements that are the furthest away from the focal point have the lowest delay and are pulsed first. Elements that are the closest have the largest delay and are pulsed last. Eventually, all the pulses will converge at a single point where the intensity of all the pulses is combined.

Beam-steering was an important method used in the linear phased array welding system in order to focus ultrasound through water, copper, and steel. Very specific time delays had to be calculated to properly image through the 3 layers.

The data acquired from phased arrays are often represented as B-scans and C-scans. B-scans are a combination of A-scans which form a cross-section view of the sample. Every column in a B-scan represents a single A-scan acquired from different points along a line. In Chapter 4, B-scans of the welding process are analyzed in detail. An example of a welding B-scan along with a corresponding schematic can be seen in Figure 4.3.1. C-scans are a two-dimensional presentation of data displayed as a top view. An entire area of a sample is scanned and for every point scanned, an amplitude is

extracted. These amplitudes are then combined forming a C-scan. C-scans are used as a method to investigating spot welds in section 4.2. of this thesis.

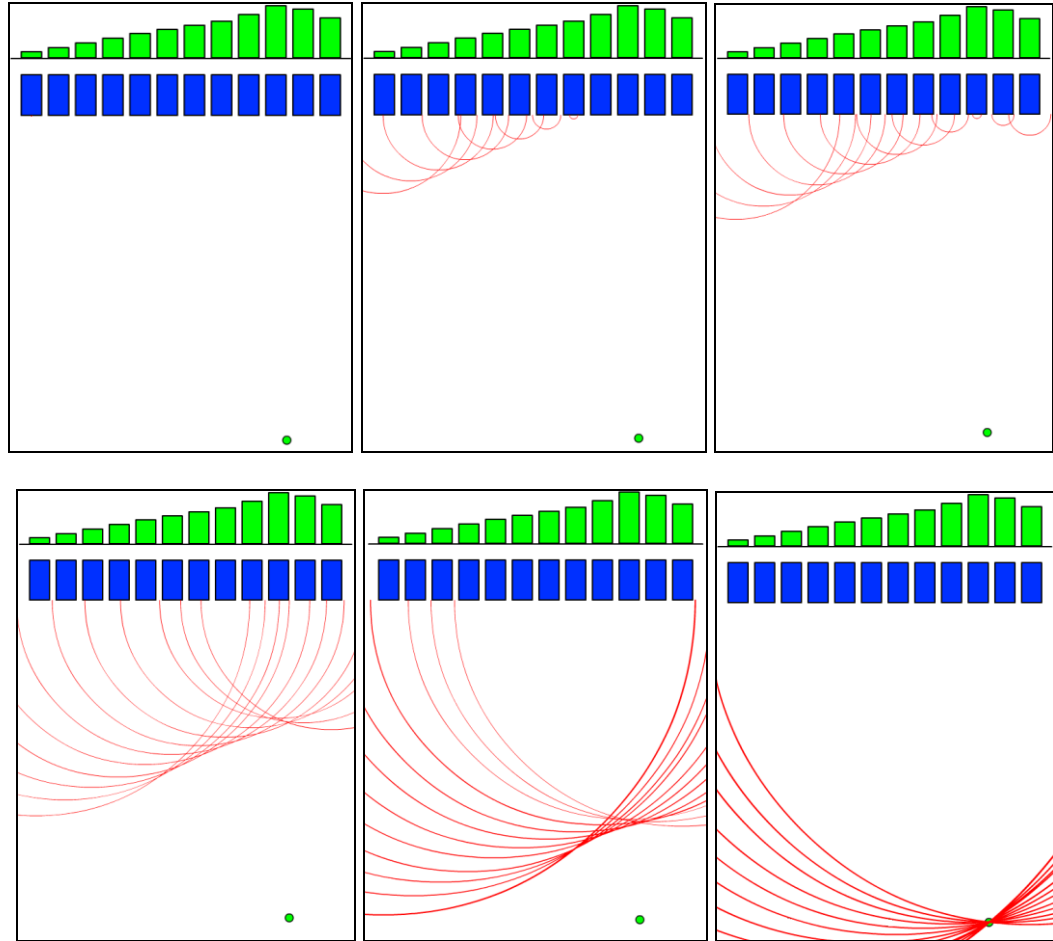


**Figure 2.5.1. Beam-steering example.**

## CHAPTER 3

### DESIGN AND METHODOLOGY

#### 3.1. Focusing Through Different Media & Snell's Law

Beam-steering presented in section 2.5. is a very important technique used in phased arrays. For the resistance spot welding application, beam-steering using a phased array transducer is not as trivial due to having to steer through water, copper, and steel. Snell's law [13], is a formula which describes the relationship between the angles of incidence and refraction, when referring to light or other waves such as sound passing through a boundary between two different isotropic media. For this welding application, the boundaries are between water and copper and between copper and steel. The formula for Snell's law is shown in Eqn. 3.1.1. where  $\theta$  is the angle measured from the normal,  $v$  is the speed of sound in the respective medium and  $n$  is the refractive index of the respective medium. A visual representation of Snell's Law is shown in Figure 3.1.1.

$$(Eqn. 3.1.1.) \quad \frac{\sin(\theta_1)}{\sin(\theta_2)} = \frac{v_1}{v_2} = \frac{n_2}{n_1}$$

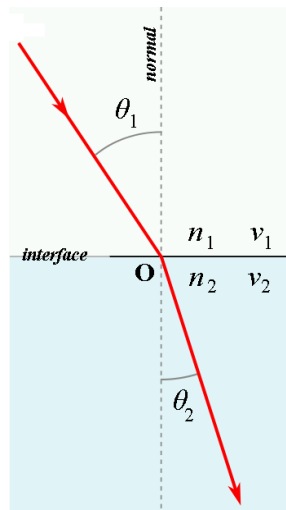


**Figure 3.1.1. Snell's law with  $v_2 < v_1$  (image from [13]).**

In Figure 3.1.1.  $v_2$  was less than  $v_1$  which meant the refracted angle  $\theta_2$  was smaller than the incident angle  $\theta_1$ . In the spot welding setup however, the speed of sound in water (1480 m/s) is much lower than the speed of sound in copper (4660 m/s) and steel (5900 m/s). In Figure 3.1.2., the spot welding setup with a line from a single element of the transducer is shown. Since  $v_{\text{water}}$  is much lower than  $v_{\text{copper}}$ ,  $\theta_2$  can get significantly larger than  $\theta_1$ .

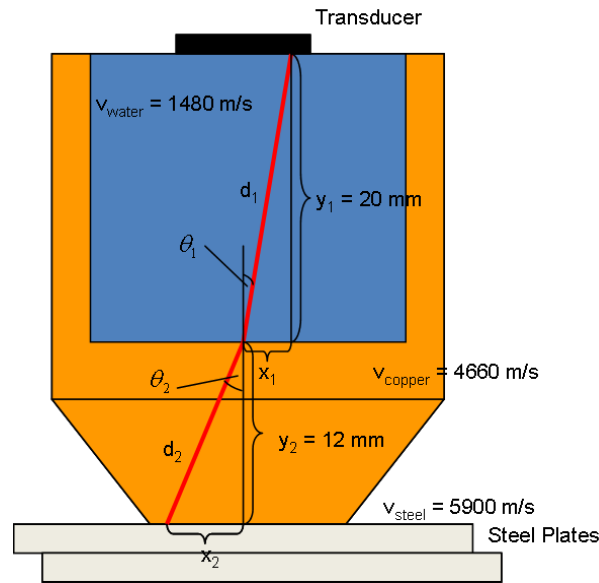


**Figure 3.1.2. Spot welding media (water, copper, steel).**

In the configuration used for this spot welding experiment, 35 lines through the steel plates were imaged. An image of the 35 lines through the weld can be seen in Figure 3.1.3. The refraction in the line can be seen between the water and copper interface. Since the speed of sound in steel was relatively close to the speed of sound in copper, they were assumed to be the same to simplify calculations. In order to image the steel plates properly, very specific time delays for transmission and reception for the 35 lines were needed. There was no analytical solution for calculating the time delays so a MATLAB

script was written to perform the many calculations. The MATLAB script can be found in Appendix A – section A.1.

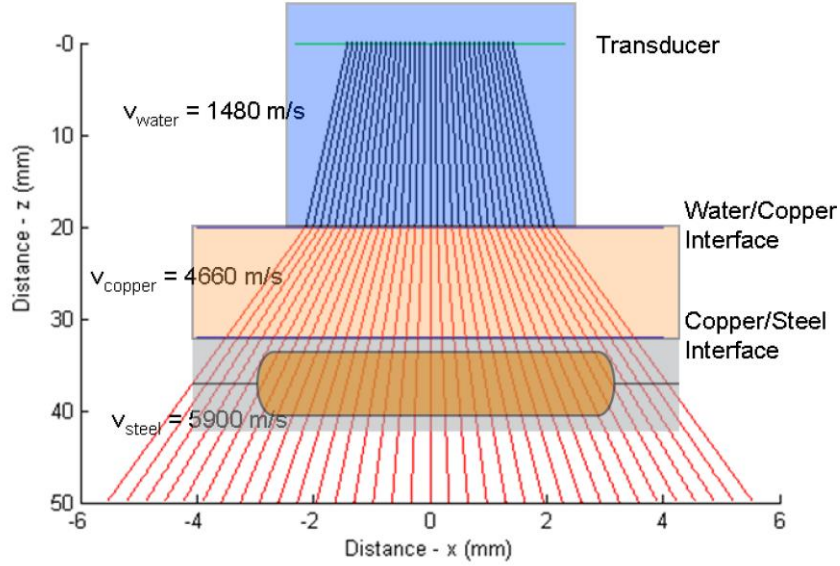


**Figure 3.1.3. Reception lines with refraction in welding setup.**

For reception each line consisted of several hundred points which all needed a delay for every transducer element, meaning 24 time delays per point. Referring to Figure 3.1.2., the distance  $y_1$  in water and  $y_2$  in copper and steel are known. The total distance along the x-direction,  $x_1 + x_2$  is also known. Combining this knowledge with Snell's law, it is possible to solve for  $\theta_1$  and  $\theta_2$  with Eqn. 3.1.2. and Eqn. 3.1.3. through an iterative approach.

$$(Eqn. 3.1.2.) \quad x_1 + x_2 = 20 \tan(\theta_1) + 12 \tan(\theta_2) = \text{known\_value}$$

$$(Eqn. 3.1.3.) \quad \frac{\sin(\theta_1)}{\sin(\theta_2)} = \frac{v_1}{v_2} = \frac{1480}{4660} = 0.3176$$

Once  $\theta_1$  and  $\theta_2$  are determined, the time of flight can be calculated using Eqn. 3.1.4.

$$(Eqn. 3.1.4.) \quad TOF = \frac{2d_1}{v_{water}} + \frac{2d_2}{v_{copper}} = \frac{2y_1}{v_{water} \cos(\theta_1)} + \frac{2y_2}{v_{copper} \cos(\theta_2)}$$

The calculated delays then need to be converted into binary files which could then be read and utilized by the ULA-OP device. This procedure is explained in more detail in section 3.3.

### 3.2. Transducer Design

Phased array technology is often used in medical and therapeutic equipment as well as in non-destructive evaluation devices. Depending on the application, ultrasonic phased arrays are designed to meet the desired requirements. These parameters include the number of elements, inter-element spacing, element size, frequency of the transducer, and the desired steering angle. In [14-15], Wooh and Shi present the effects of the various transducer parameters on the performance and behavior of the transducer and also provide guidelines on how to optimize an ultrasonic phased array. A schematic of a generic linear phased array is shown in Figure 3.2.1 with some of the parameters highlighted. The figure shows a phased array with “N” elements with an element width of “a” and a pitch of “d”. Each element is also composed of “M” point sources of ultrasound.

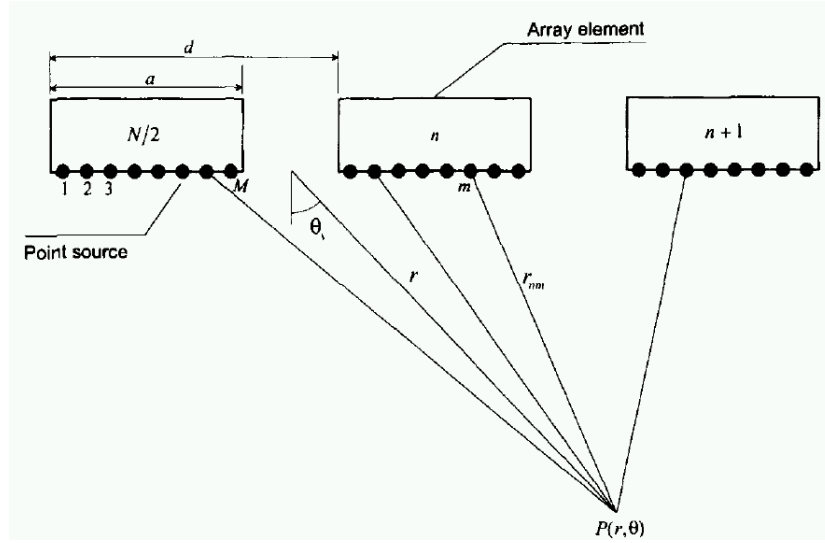


**Figure 3.2.1. Schematic of generic phased array (image from [14]).**

Wooh and Shi also present a 5-step suggested guideline for optimal transducer design as follow:

1. Select the transducer frequency and calculate the wavelength “ $\lambda$ ” for the given inspection materials.
2. Determine the lateral dimension “D” that meets the requirements of near-field length depending on the type of inspection tasks. Smaller transducers will have shorter near-field length and thus will provide an enlarged inspectable area.
3. Within the given lateral dimension “D”, make the number of elements “N” as large as allowed by the fabrication technology and the control electronics.
4. Determine the inter-element spacing  $d \approx D/N$  and the critical inter-element spacing “ $d_{cr}$ ”, If  $d < d_{cr}$ , then go to Step 5. If  $d > d_{cr}$ , grating lobes will be introduced. To remedy this, “D” should be decreased until  $d < d_{cr}$  (assuming that a maximum “N” is already chosen in Step 3. If it is

technically allowable, reduce “D”. If not, the only way to eliminate grating lobes is to decrease the frequency.

5. Select the largest possible element width “a” for the highest possible pressure in the steering direction. To obtain higher steering angle, reduce the element width.

The linear phased array transducer used in the welding setup, was not designed by the author but by another member of the same research group. The design of the linear phased array could not be done by simply following the guidelines listed above, due to the spot welding setup. Some limitations were present and had to be considered in the transducer design. The maximum aperture of the linear phased array transducer was limited by the inner diameter of the welding electrode the transducer was to be installed into. The key design specifications were to first use the largest aperture possible that would fit inside the electrode which had an inner diameter of 11. Even with an inner diameter of 11, the total aperture of the linear array ended up only being 4.75 mm due to the transducer casing. From this, the element size was minimized to allow for wider beam-steering angles, this was limited by the transducer manufacturing process used by Doppler Electronics. Then a frequency was selected which would still allow the probe to steer at the angles required. The elevation was also maximized to increase the power of each individual transducer element.

The specifications of the linear phased array probed used in the welding system can be found in Table 3.2.1.



Specification	Value
Center frequency (-6 dB)	10 MHz $\pm$ 10%
Number of elements	24
Elementary pitch	0.2 mm
Inter-element spacing	0.05
Element size	0.15 mm
Elevation	4.0 mm
Bandwidth (-6 dB)	> 60%
Homogeneity in sensitivity	Mean $\pm$ 3 dB and Standard dev. < 1dB
Inter-element coupling between elements	< -30 dB
Acoustic matching	Immersion (water)

**Table 3.2.1. Linear phased array specifications.**

### 3.3. ULA-OP Device

In collaboration between the University of Windsor and the University of Florence, the ULA-OP device was used to control the phased array transducer. ULA-OP stands for Ultrasonic Advanced Open Platform and is completely developed at the University of Florence [16]. The ULA-OP has many features which were essential for the welding application. In the welding setup, having to focus ultrasound through different media (water, copper, steel), very specific time delays were needed so a device which was open source and completely programmable was important. Other commercial devices lacked the flexibility needed for this research application.

The ULA-OP consists of a metal casing with dimensions 34 x 23 x 14 cm which can be connected to a computer and an ultrasonic probe. Dedicated software has been developed to run with the ULA-OP device. The inside of the metal casing features 2 main

boards, a digital board and an analog board. This setup can be seen in Figure 3.3.1. and an overview of the main features of the ULA-OP is listed in Table 3.3.1.

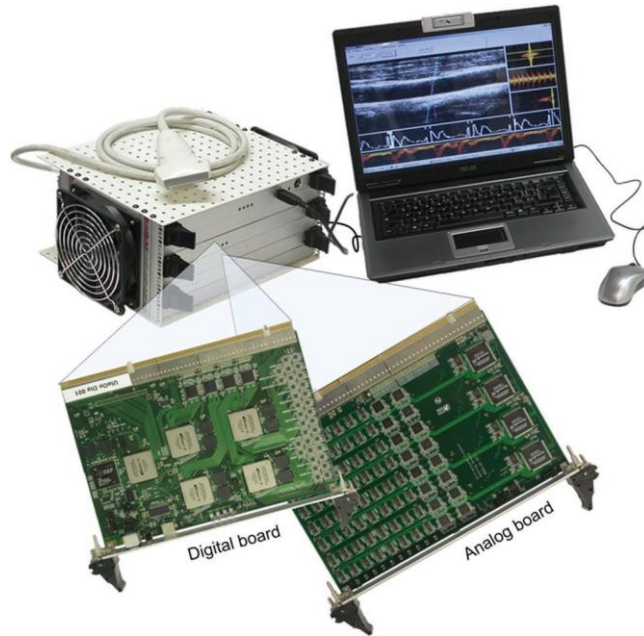


**Figure 3.3.1. ULA-OP overview (image from [16])**

Specification	Value
General features	<ul style="list-style-type: none"> <li>➤ Open platform</li> <li>➤ 64 independent TX/RX channels</li> <li>➤ Size: 34 x 23 x 13 cm; Weight: 5 kg</li> <li>➤ Power consumption &lt; 90W</li> </ul>
Transmitter	<ul style="list-style-type: none"> <li>➤ 64 square wave pulsers</li> <li>➤ Max output voltage: 150 Vpp</li> <li>➤ Frequency: 1 to 16 MHz</li> </ul>
Receiver	<ul style="list-style-type: none"> <li>➤ Input noise: 2nV / <math>\sqrt{\text{Hz}}</math></li> <li>➤ Bandwidth: 1 to 16 MHz</li> <li>➤ Analog gain: 6-46 dB with programmable TGC</li> <li>➤ 12 bit @ 50 MSPS ADCs</li> </ul>

Beam-former	➤ Programmable apodization and delays (dynamic focusing)
Processing modules	➤ Coherent demodulation, band-pass filtering, decimation, B-mode, multigate spectral Doppler, vector Doppler, custom modules
Storage capabilities	➤ Up to 1 GB for RF data (pre or post beam- formed) ➤ Up to 512 MB for baseband data ➤ Fast data streaming toward high capacity storage units (HD)
Software tools	➤ Beam Planner, Configuration Editor, Real-time Module, Video Browser, RF viewer.

**Table 3.3.1. ULA-OP main features (from [16]).**

The software provided with the ULA-OP device is able to provide real-time imaging of the results on configurable display windows. In the software, the user is also able to set and change parameters affecting real-time operations and to download the acquired data using the control interface. An example of the display window and control interface for the spot welding acquisitions can be seen in Figure 3.3.2.

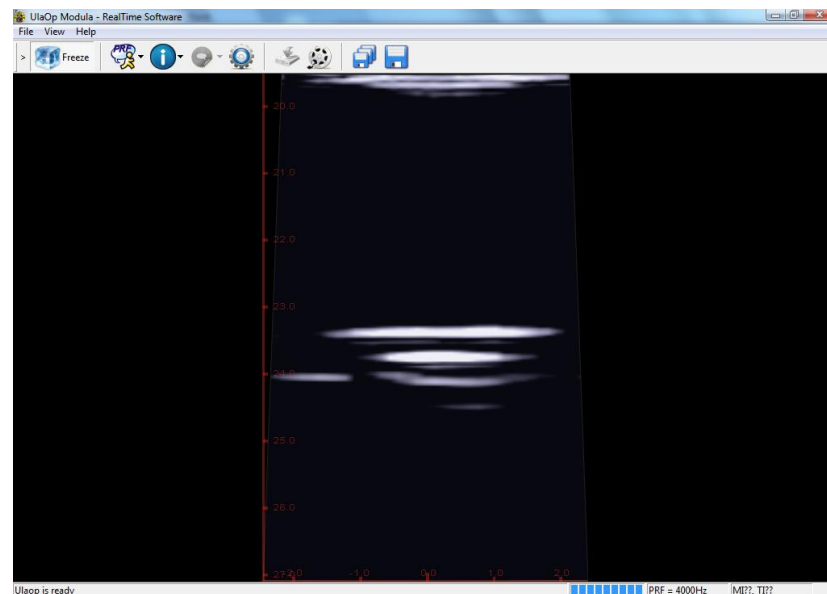


**Figure 3.3.2. ULA-OP module – Real-time software.**

An important feature of the ULA-OP device was to be able to program it with custom time delays for beam-forming/steering. Beam-steering was covered in section 2.4. Custom time delays for transmission and reception in the welding application was very important due the presence of three different media in which sound needed to travel through. The procedure used to calculate the time delay tables was presented in detail in section 3.1. Once the time delay tables for transmission and reception were calculated, they needed to be converted into binary files which could then be read and utilized by the ULA-OP device. MATLAB scripts provided by the University of Florence were used to perform the conversion. The script for generating \*.bft files for transmission delays can be found in Appendix A – section A.2. and the script for generating \*.bfr files for reception can be found in Appendix A – section A.3. Section 4.3.5. of the ULA-OP manual [17] explains this procedure in more detail.

In order to tell the ULA-OP device which mode to run in and which transmission and reception files to use, a configuration \*.cfg text file is needed. The configuration file specifies most of the parameters contributing to the mode and links to other files where needed. The configuration file used in the linear phased array welding setup can be found in Appendix A – section A.4. Another important file is the ULA \*.ula text file. This ULA file is linked to the configuration file. Inside the ULA file, the transmission and reception parameters are found and links to the \*.bft and \*.bfr time delay binary files. The ULA file used in the linear phased array welding setup can be found in Appendix A – section A.5.

The specialized electronics in the ULA-OP allowed for a high pulse repetition frequency (PRF) which was needed in order to record the entire welding process which occurs in less than 300 ms. The PRF used for the linear phased array welding system was

15 kHz, meaning a pulse was sent every 66.7  $\mu$ s. The ULA-OP also has the ability to use many different probes, making it flexible and suitable if other ultrasonic phased array are implemented in future projects. Another important feature of the ULA-OP was to begin and continue imaging and storing data when a trigger signal is being sent to the device. By connecting the weld gun trigger to the ULA-OP device, the ULA-OP would begin acquiring data as soon as the welding process began and continued to acquire data until welding was complete.

### 3.4. Transducer Housing Design

Before the transducer could be used in welding, a custom housing was needed to mount it to the weld gun and also prevent it from being damaged from heat or electric current. The initial designs were made in Google Sketchup and then sent to Centerline Limited where one of the engineers optimized the design and made sure it followed all of the operating and safety requirements of a welding electrode. One of the key focuses of the design was to integrate the existing water lines so an external water source was not needed. Since the linear phased array transducer was designed to be as large as possible and still fit inside welding electrode, there was no longer sufficient space for water to flow through. The water needed to be routed out of the electrode, through the caps and then back into the electrode water drain. Initially, water lines would be tapped directly into the welding caps as shown in Figure 3.4.1. An external tube would be used to connect the water lines between the electrode and the cap. The distance of the water channel between the transducer and the inside of the electrode cap had to be within 15 mm to 20 mm. A protective sleeve for the transducer itself was needed to protect the

transducer from electric current flow in the system. The initial design had a one-piece sleeve with an o-ring to keep it from moving.

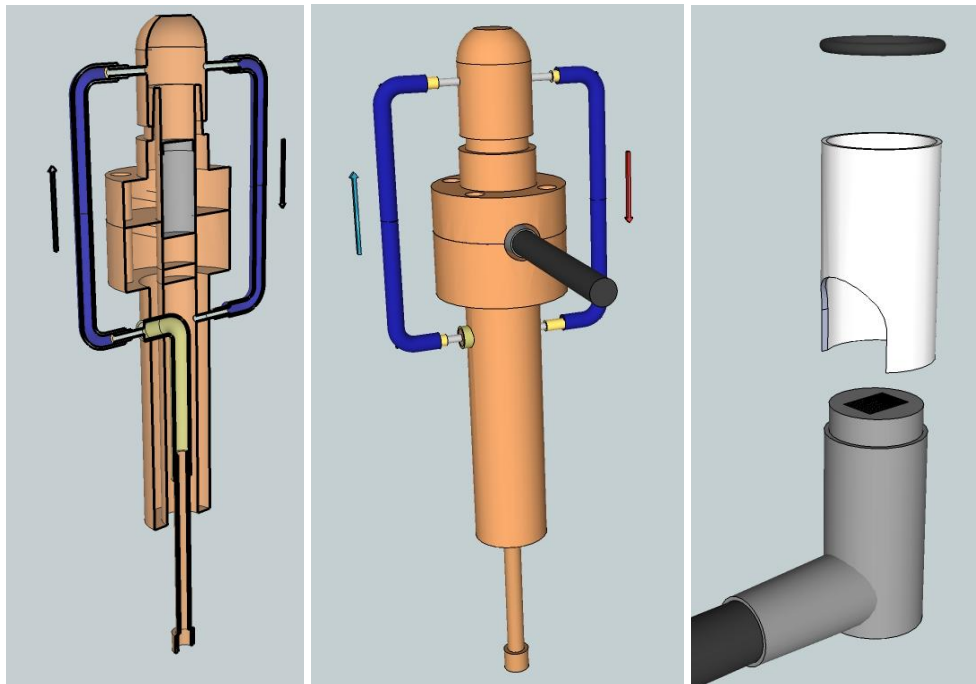


**Figure 3.4.1. Initial transducer housing design.**

After working closely with Centerline Limited, a few design changes and optimizations were agreed upon. One welcomed change was to tap the water lines directly into the welding electrode directly above the surface of the transducer instead of tapping into the caps as shown in Figure 3.4.2. This saved the trouble of having to make custom caps for the welding setup. To ensure water would stay inside the water channel, the drain had a smaller diameter than the water supply. The housing would then sit on a bent adapter to be attached to the weld gun. The sleeve for the transducer ended up being two pieces with two o-rings. One o-ring to ensure the transducer would not slide from the sleeve and one to ensure the sleeve would not slide from the housing.

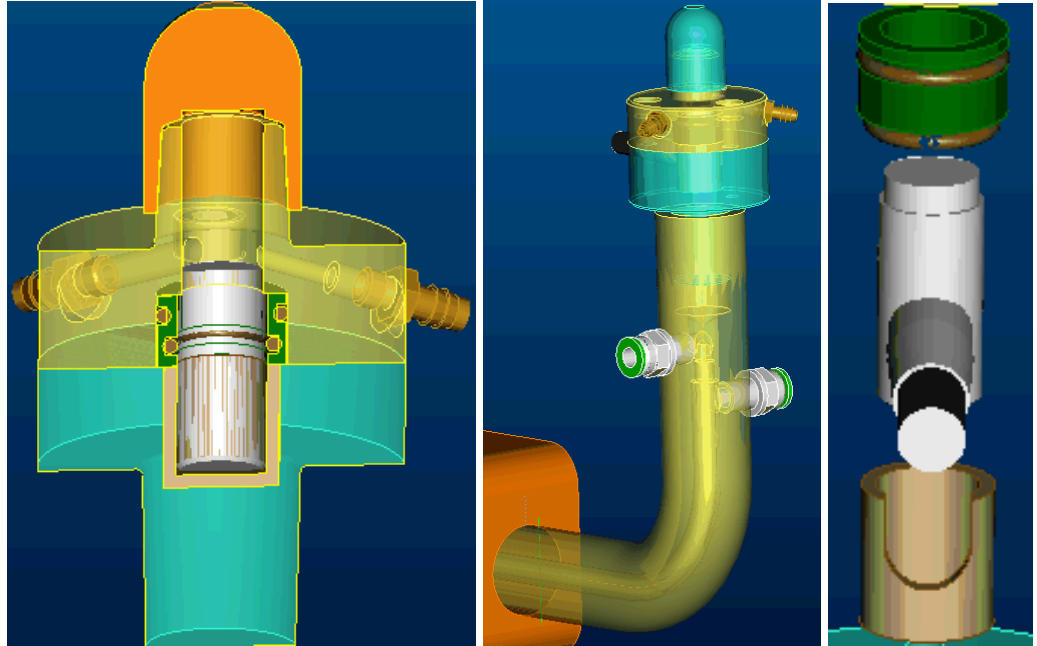


**Figure 3.4.2. Final transducer housing design.**

The final design was then manufactured by Centerline and the transducer was installed inside the housing as shown in Figure 3.4.3.



**Figure 3.4.3. Manufactured bent adapter (left) and assembled housing (middle & right).**

The water tubes could then be attached and the bent adapter could be attached to the weld gun as shown in Figure 3.4.4. With the final assembly and the ULA-OP for controlling the linear phased array transducer, the spot welding process could be monitored and recorded in real-time.



**Figure 3.4.4. Final assembly.**

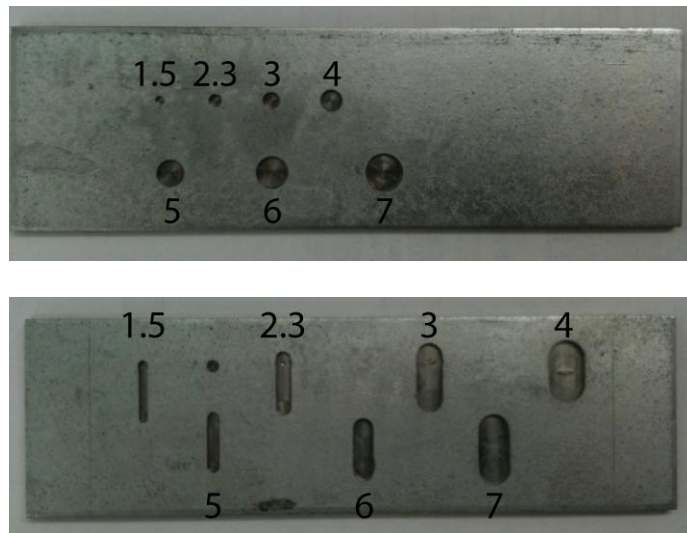


## CHAPTER 4

### ANALYSIS OF RESULTS

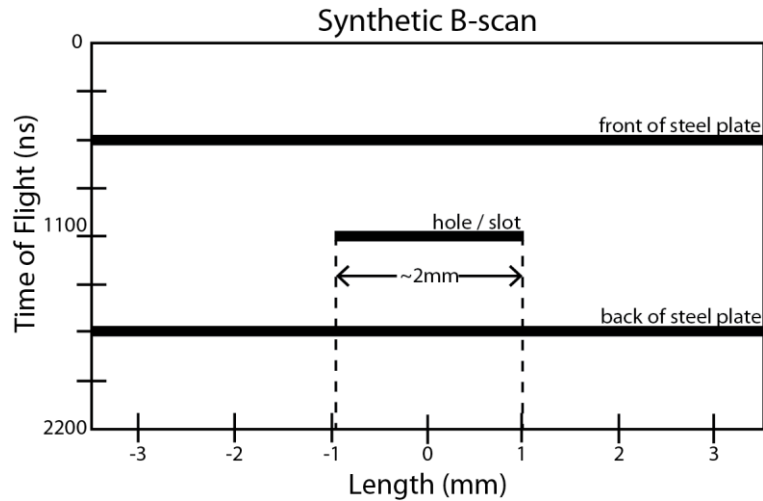
#### 4.1. Preliminary Results

Holes and slots were drilled into 2.5 mm thickness steel plates. The holes and slots were drilled in 1 mm deep with seven different diameters and widths ranging from 1.5 mm to 7 mm to simulate various nugget sizes. Initially, only holes were being used but it was challenging to ensure the hole was perfectly centered along the probe's steering path while being squeezed by the weld gun. Slots were then used to eliminate the need to center the slot along the probe's steering path. The plates are shown in Figure 4.1.1. with the diameter or slot width labeled in millimeters. Ultrasonic beams were steered through the water channel and the copper cap, to the steel plates to simulate the welding setup. B-scans of the holes and slots were imaged.



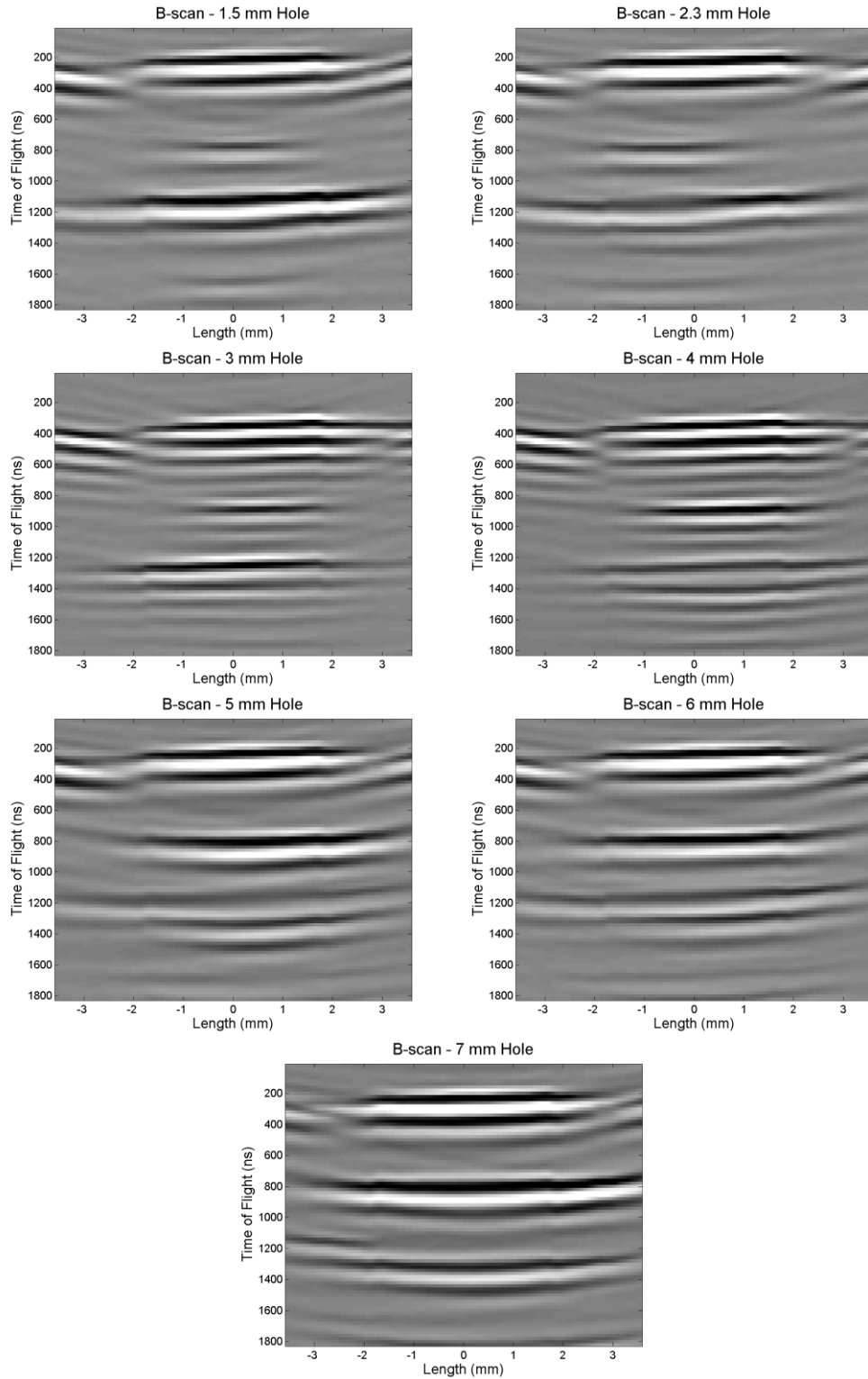
**Figure 4.1.1. Plates with holes (top) & slots (bottom).**

Figure 4.1.2. shows a synthetic B-scan of a hole or slot. In the figure, the size of the hole / slot is about 2 mm.



**Figure 4.1.2. Synthetic B-scan of a 2 mm hole / slot.**

The B-scans acquired for the holes are shown in Figure 4.1.3., and the slots shown in Figure 4.1.4. In this setup, a maximum of 7.1 mm in the steel can be monitored. As mentioned above, centering the holes along the probe's path was a difficult task so in many cases, the size of the hole on the B-scan might appear slightly smaller than the actual size. Looking at both the B-scans for the holes and slots, it is very easy to see that as the size of the hole or slot increased, the reflections of the hole or slot also got longer. Determining an exact measurement from the B-scans however, is not as obvious. Since the slots provided more accurate images of slot sizes, slots were the focus of the analysis.



**Figure 4.1.3. B-scans of holes (1.5 mm to 7 mm).**

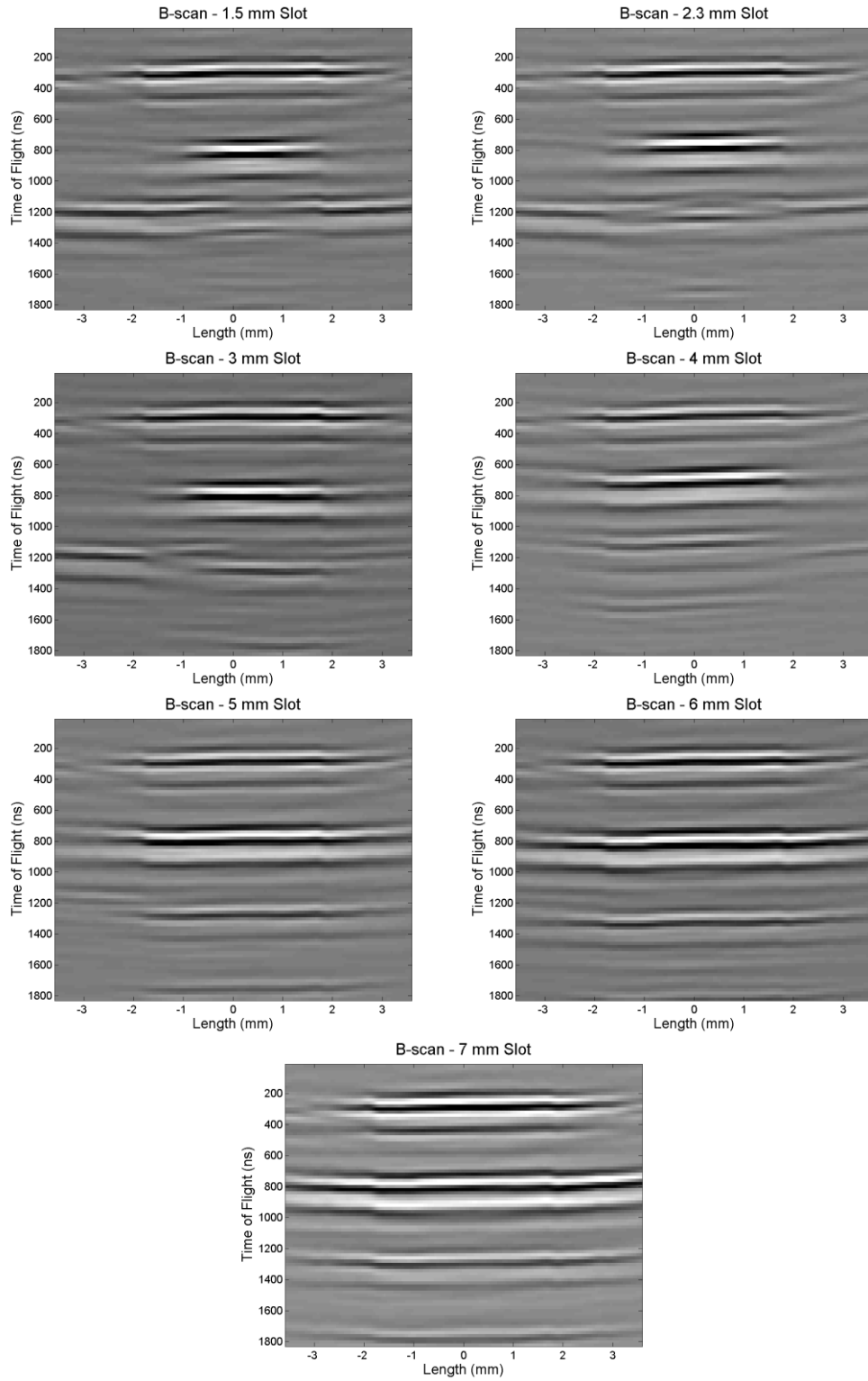


**Figure 4.1.4. B-scans of slots (1.5 mm to 7 mm).**

Some image processing techniques were used to help obtain a more accurate measurement of the slots. The image and signal processing was performed in MATLAB. The MATLAB code for determining slot sizes can be found in Appendix B – section B1. The original B-scan acquired from the ULA-OP device contained radio frequency data. Using the ULA-OP device, it is also possible to obtain demodulated data using demodulators available on the device to recover the original signal. In the following procedure only radio frequency data was recorded from the ULA-OP device. This gave the flexibility to apply demodulation after the acquisition and using MATLAB to select a filter which best suited the application. In Appendix B of the ULA-OP manual [17], a table providing recommended coefficients for a low pass filter based on the central frequency of the transducer and the bandwidth of the transducer can be found. This table was used as a guideline for the low pass filter used in the procedure.

Considering the sampling theorem [18], the radio frequency data was multiplied by the expression in Eqn. 4.1.1., where  $f_o$  is the center frequency of the transducer and  $t$  is time. In this case, time for a sample is equal to the number of the sample ( $n$ ) divided by the sampling frequency ( $F_s$ ). This procedure performs a frequency shift that shifts the signal to the baseband.

$$(Eqn. 4.1.1) \quad e^{j2\pi f_o t} = e^{j2\pi f_o \frac{n}{F_s}}$$

Once the signal is shifted to the baseband, a low pass filter is used to filter out unwanted signals. Since the linear array transducer had a central frequency of 10 MHz with a 60% bandwidth (6dB) and was sampled with a sampling frequency ( $F_s$ ) of 50 MHz, the filter included a pass band between 0 and 3.75 MHz (-3dB) and an attenuation band between 7.5 MHz and 25 MHz ( $F_s/2$ ) with 60dB of attenuation. Functions are

available on MATLAB to create filters simply by entering the parameters for the pass band and attenuation band. The frequency response of the filter is shown in Figure 4.1.5. The B-scan containing radio frequency data and the B-scan containing the demodulated data are shown in Figure 4.1.6.

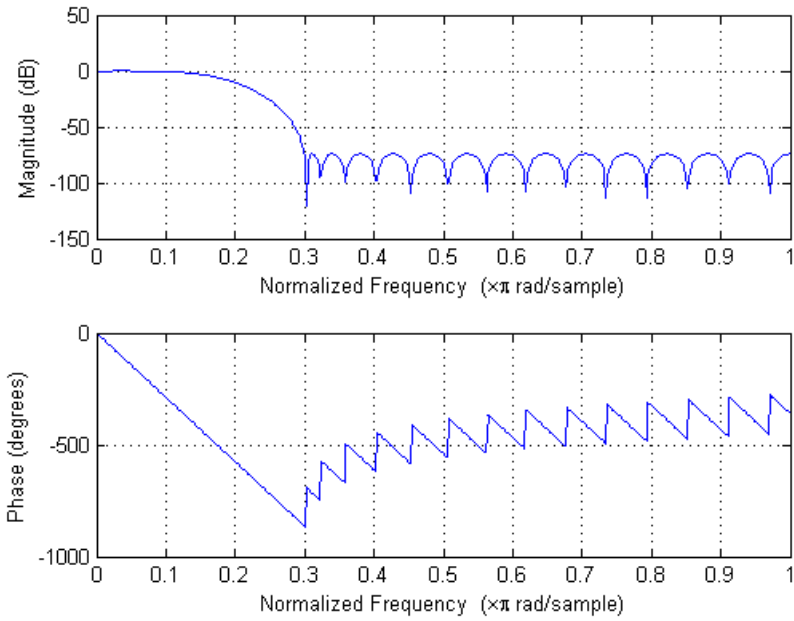


**Figure 4.1.5. Frequency response of finite impulse response (FIR) Filter**

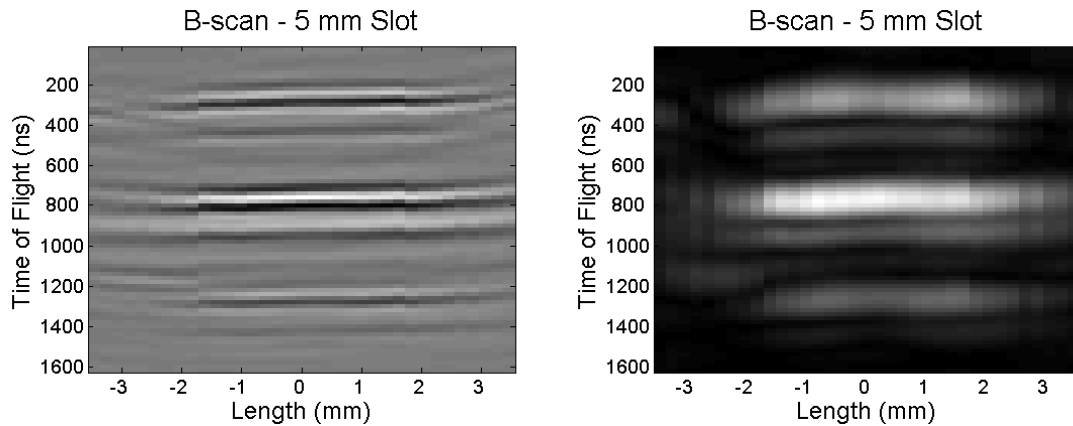


**Figure 4.1.6. B-scans w/ radio frequency data (left) & demodulated data (right).**

After demodulation, cubic interpolation is also applied to the B-scan to increase the number of data points in both the x and y directions. On the interpolated image, a

window which surrounds the entire slot is used. The window is 21 pixels high and 137 pixels long covering the entire length of the x axis. In every column of the window, the maximum amplitude is extracted and is used to plot the maximum amplitude along the slot. The interpolated B-scan with the window and the maximum amplitude plot is shown in Figure 4.1.7.

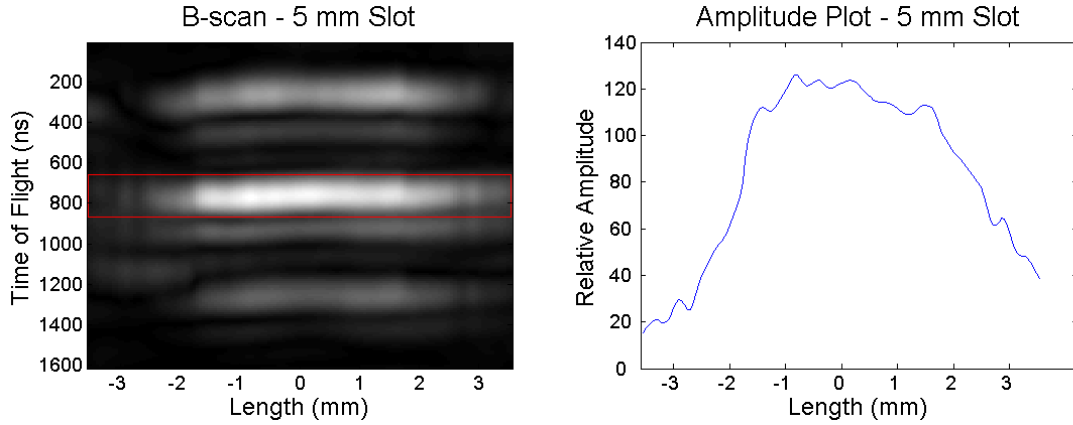


**Figure 4.1.7. Interpolated B-scan with window (left) & amplitude plot (right).**

From the amplitude plot, two halves of a Gaussian curve are fit to the amplitude plot using the least squares fitting [19] method. A Gaussian can be represented as a function shown in Eqn. 4.1.2. In this equation, A represents the amplitude of the curve's peak, x is the x-coordinate of a point along the curve, m is the position of the center of the peak, and  $\sigma$  is the distance between the flex point and the middle point of the curve. A visual representation is provided in Figure 4.1.8 where  $A = 2$ ,  $m = 5$ , and  $\sigma = 3$ .

$$(Eqn. 4.1.2.) \quad f(x) = Ae^{-\left(\frac{x-m}{\sigma}\right)^2}$$

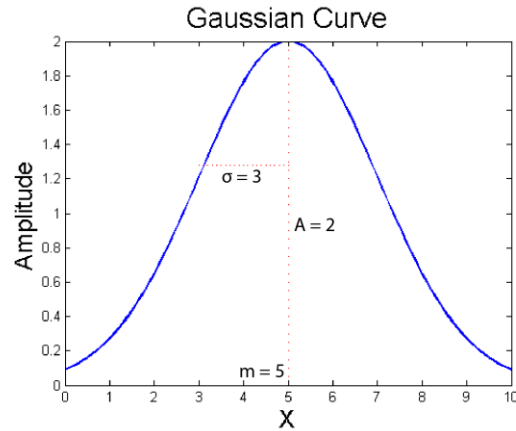


**Figure 4.1.8. Gaussian curve.**

Figure 4.1.9. shows the Gaussian fit on the amplitude plot. From each half of the Gaussian curve, the flex is taken as a reference point, and based on where the flex lies, a correction is applied. A correction is needed due to the non-linearity of the acquired image in the x-direction caused by the refraction of sound waves in steel. The corrected point is then considered a boundary where a slot is present or not present. The number of pixels between the two corrected flex points is then known and can be used to calculate the slot size by simply multiplying the number of pixels by the length per pixel. The processing for the 5 mm slot is shown and the slot was calculated to be 5.02 mm by the algorithm presented.

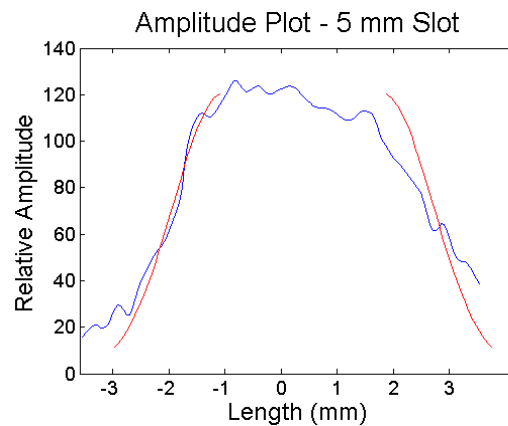


**Figure 4.1.9. Amplitude plot with Gaussian fit.**



The Gaussian fitting for the other slots are shown in Figure 4.1.10 with the calculated sizes of the slots using the algorithm presented in Table 4.1.1.

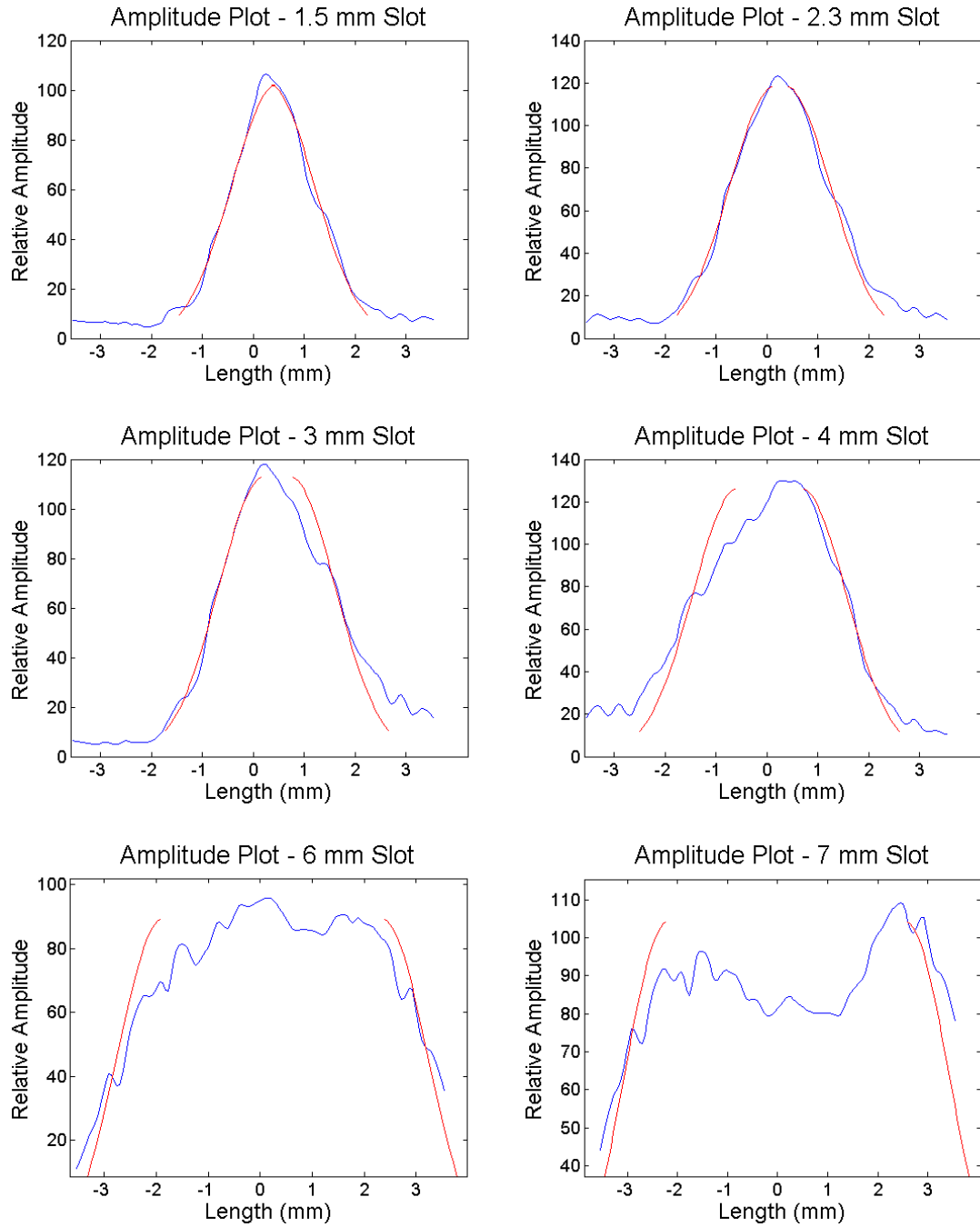


**Figure 4.1.10. Gaussian fit on several slot sizes.**

<b>Actual Size (mm)</b>	<b>Calculated Size (mm)</b>	<b>Error (mm)</b>
1.5	2.18	+ 0.68
2.3	2.52	+ 0.22
3	2.82	- 0.18
4	3.51	- 0.49
5	5.02	+ 0.02
6	6.29	+ 0.29
7	6.78	- 0.22

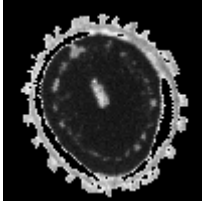
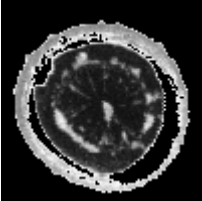
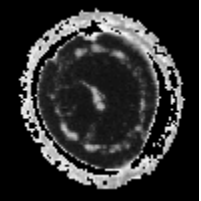
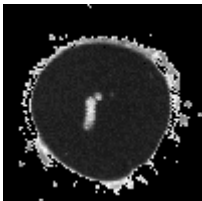
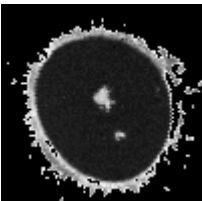
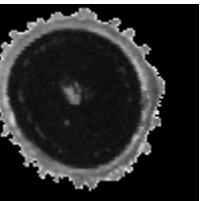
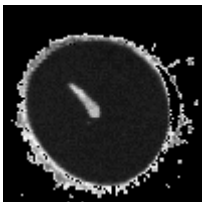
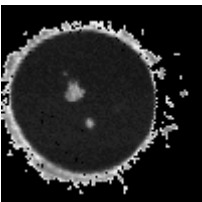
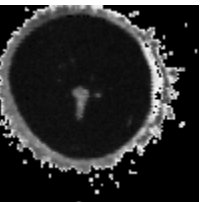
**Table 4.1.1. Calculated Slot Sizes.**

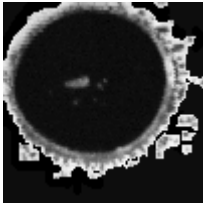
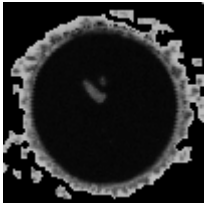
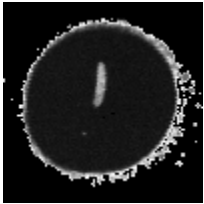
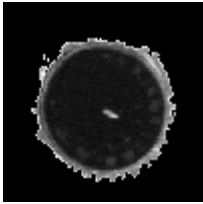
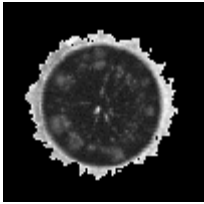
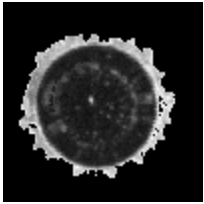
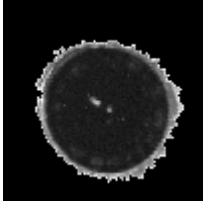
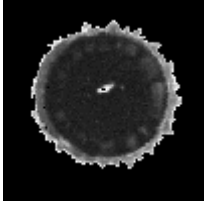
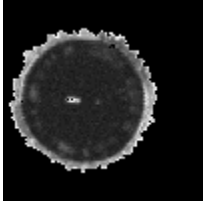
The calculated sizes ranged in error from 0.02 mm to 0.68 mm. It was difficult to get an accurate measurement of the 1.5 mm slot due to the large beam width in steel (~3mm). Overall the calculation method is able to distinguish between slots which were different in size by only 1 mm.

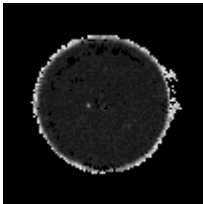
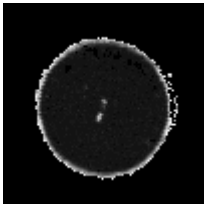
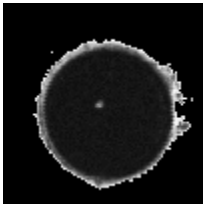
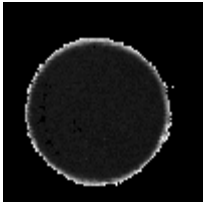
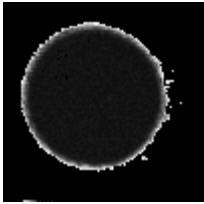
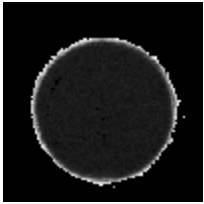
#### 4.2. Off-line Spot Weld Evaluation Using Existing Methods

Several welds using various parameters were performed and recorded with the linear phased array system. Two sets of welds were performed. The first set used two welding electrode caps with the same tip face diameter of 8 mm. In this set, welding currents between 9.5 kA and 11 kA were used. The second set used one welding electrode cap with a face diameter of 8 mm to maximize the viewing window for the transducer and a 4.8 mm tip face diameter for the second electrode cap. The smaller tip face diameter leads to a higher current density for the same current when compared to a larger tip face, meaning lower currents were needed to create similar welds to set one. In set two, welding currents between 8 kA and 9.5 kA were used.

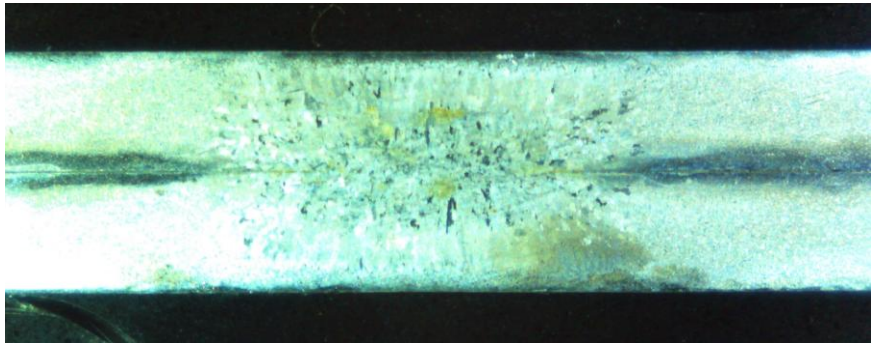
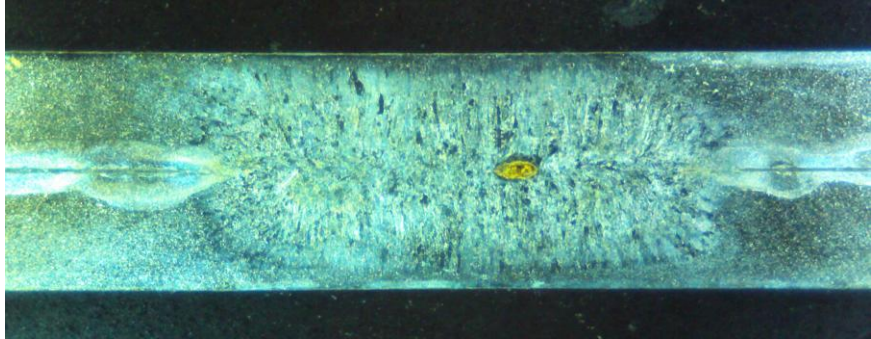
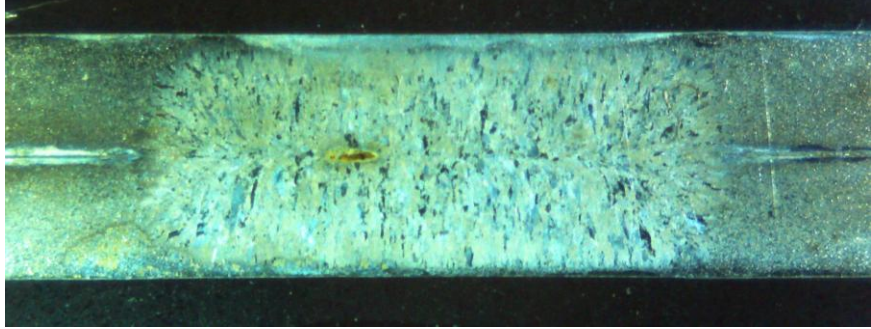
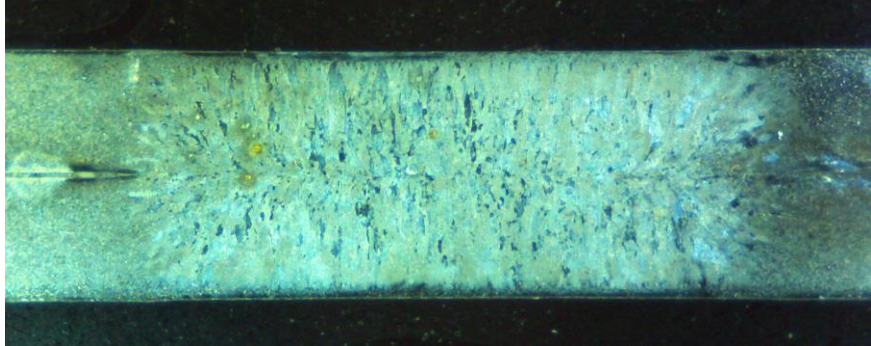
To understand and verify the geometry and properties of these welds, traditional off-line inspection methods were used, including acoustic imaging, peel tests, and cross-sections. For every current level selected, 3 spot welds labeled a, b, and c were performed and recorded using the ULA-OP device. Once completed, every weld was imaged again using an acoustic microscope to produce C-scans with a 50 MHz transducer. These C-scans are shown in Table 4.2.1. where each square represents a 10 mm by 10 mm region. The weld nugget diameters and size of the voids are also shown in Table 4.2.1. Cross-sections and peel tests were each performed on one weld for every current level. The welds labeled “a” were cross-sectioned and the welds labeled “b” were peeled. Images of the Cross-sections along with the measured diameter can be found in Table 4.2.2. and the measured nugget diameters from the peel tests can be found in Table 4.2.3. These results were used as a reference for the images acquired with the linear phased array system.

Current	Set	a				b				c			
9.5 kA	1												
		Nugget size (mm)		Void size (mm)		Nugget size (mm)		Void size (mm)		Nugget size (mm)		Void size (mm)	
		X	Y	X	Y	X	Y	X	Y	X	Y	X	Y
		3.59	2.36	0.97	1.50	2.36	2.42	0.53	0.82	2.58	3.68	0.62	1.23
10 kA	1												
		Nugget size (mm)		Void size (mm)		Nugget size (mm)		Void size (mm)		Nugget size (mm)		Void size (mm)	
		X	Y	X	Y	X	Y	X	Y	X	Y	X	Y
		6.12	6.04	0.86	1.89	5.93	6.50	1.12	1.13	6.45	6.78	0.98	1.12
10.5 kA	1												
		Nugget size (mm)		Void size (mm)		Nugget size (mm)		Void size (mm)		Nugget size (mm)		Void size (mm)	
		X	Y	X	Y	X	Y	X	Y	X	Y	X	Y
		6.59	6.78	1.56	1.89	6.89	6.85	1.01	1.06	7.09	7.14	0.97	1.10

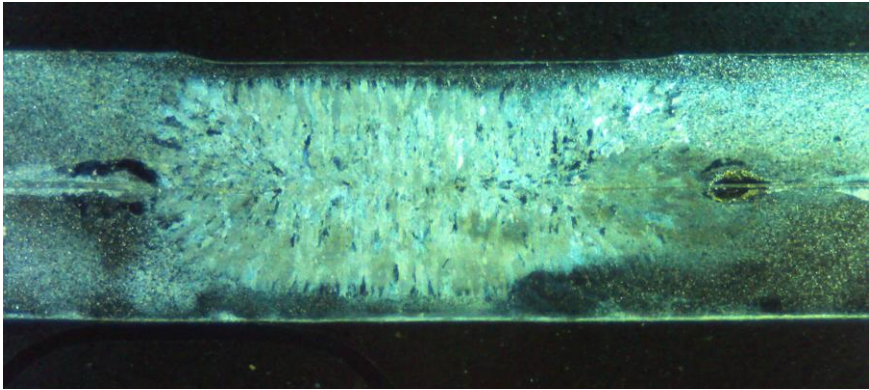
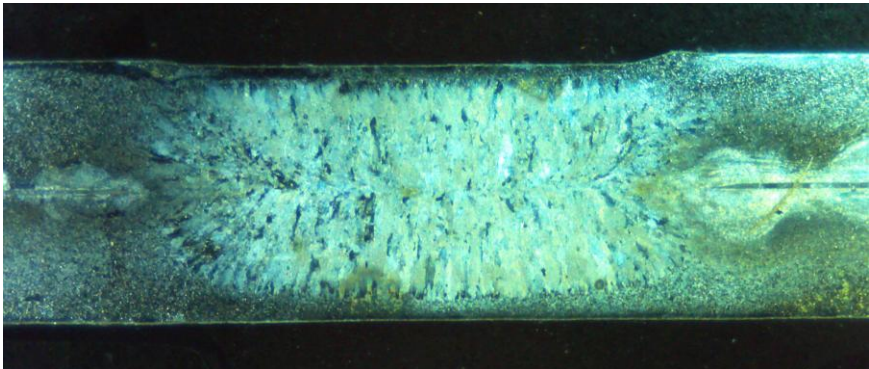
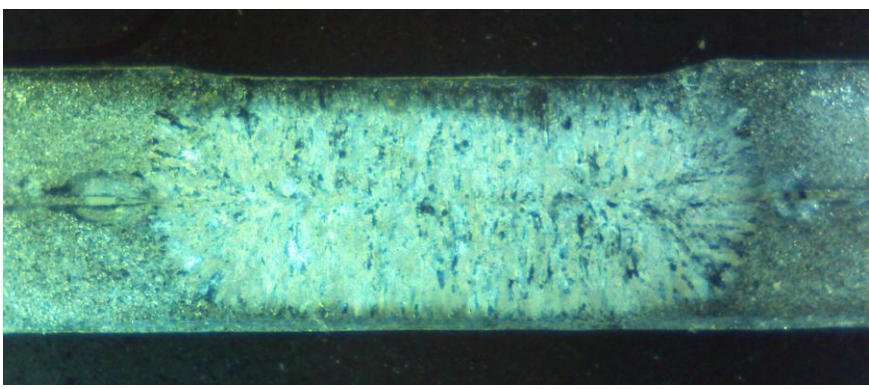
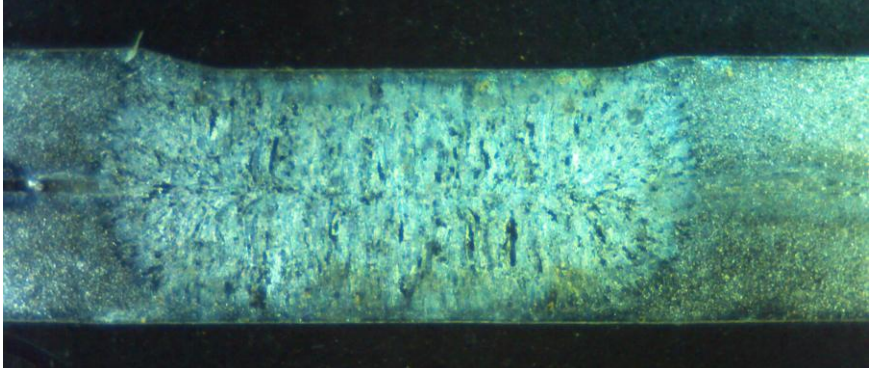
11 kA	1												
		Nugget size (mm)		Void size (mm)		Nugget size (mm)		Void size (mm)		Nugget size (mm)		Void size (mm)	
		X	Y	X	Y	X	Y	X	Y	X	Y	X	Y
		7.56	7.01	1.19	0.57	7.00	7.34	1.08	1.17	7.36	7.34	0.60	2.14
8 kA	2												
		Nugget size (mm)		Void size (mm)		Nugget size (mm)		Void size (mm)		Nugget size (mm)		Void size (mm)	
		X	Y	X	Y	X	Y	X	Y	X	Y	X	Y
		3.73	3.75	0.84	0.49	3.30	3.41	0.40	0.44	3.52	3.37	0.29	0.37
8.5 kA	2												
		Nugget size (mm)		Void size (mm)		Nugget size (mm)		Void size (mm)		Nugget size (mm)		Void size (mm)	
		X	Y	X	Y	X	Y	X	Y	X	Y	X	Y
		4.55	4.64	0.57	0.55	3.92	4.32	0.84	0.46	4.16	4.49	0.82	0.37

9 kA	2												
		Nugget size (mm)		Void size (mm)		Nugget size (mm)		Void size (mm)		Nugget size (mm)		Void size (mm)	
		X	Y	X	Y	X	Y	X	Y	X	Y	X	Y
		6.28	6.19	0.15	0.24	5.93	6.26	0.35	0.44	6.04	6.34	0.15	0.24
9.5 kA	2												
		Nugget size (mm)		Void size (mm)		Nugget size (mm)		Void size (mm)		Nugget size (mm)		Void size (mm)	
		X	Y	X	Y	X	Y	X	Y	X	Y	X	Y
		6.45	6.65	-	-	6.34	5.52	-	-	6.54	6.70	-	-

**Table 4.2.1. Acoustic Microscope C-scans (10 mm x 10 mm) of Welds with Measurements.**

Weld	Nugget Diameter (mm)	Cross-section
9.5 kA-a Set 1	3.55	
10 kA-a Set 1	5.92	
10.5 kA-a Set 1	6.76	
11 kA-a Set 1	7.46	



9.5 kA-a Set 2	4.12	
9.5 kA-a Set 2	5.22	
9.5 kA-a Set 2	6.52	
9.5 kA-a Set 2	6.78	

**Table 4.2.2. Cross-sections of welds.**



Weld	Set	Nugget Diameter	
		X (mm)	Y (mm)
9.5 kA-b	1	2.27	2.34
10 kA-b	1	5.49	6.23
10.5 kA-b	1	6.49	6.75
11 kA-b	1	6.40	7.2
8 kA-b	2	3.03	3.13
8.5 kA-b	2	3.79	3.89
9 kA-b	2	5.58	5.87
9.5 kA-b	2	5.76	6.4

**Table 4.2.3. Peel test nugget diameters.**

#### 4.3.Real-time Spot Weld Monitoring

The primary objective of this project was to extend upon the existing single element in-line system. The linear phased array system had the ability to monitor a cross-section through a spot weld as opposed to a single line through the center of a spot weld monitored by the existing single element in-line system. With the linear phased array mounted in the custom transducer housing and attached to the weld gun, the welding process could be monitored in real time. Using the ULA-OP device, the transducer could be controlled very precisely in order to steer and focus the ultrasonic beam.

In each weld, 35 lines through the weld were recorded for the duration of welding. Figure 3.1.3. shows a visual representation of the 35 lines in the weld setup. With the data recorded, B-scans and M-scans could be formed to give a nice visual representation of the entire welding process. A pulse repetition frequency of 15 kHz was used in this experiment, meaning each A-scan was acquired in 66.7  $\mu$ s and a single B-scan was

acquired in 2.33 ms. M-scan formation was covered in section 2.4. and B-scan formation was covered in section 2.5. Figure 4.3.1. shows the correlation between a physical weld and a B-scan by highlighting some key areas and reflections of the weld.

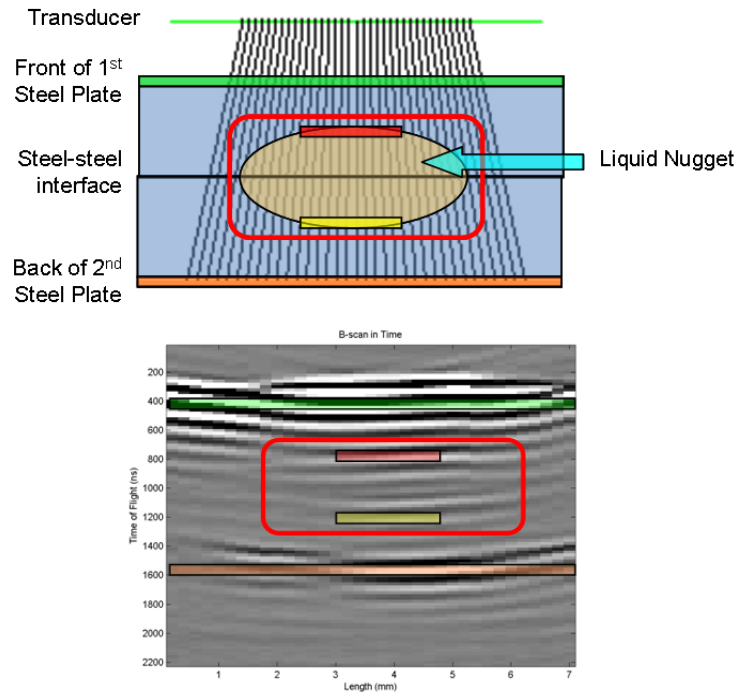
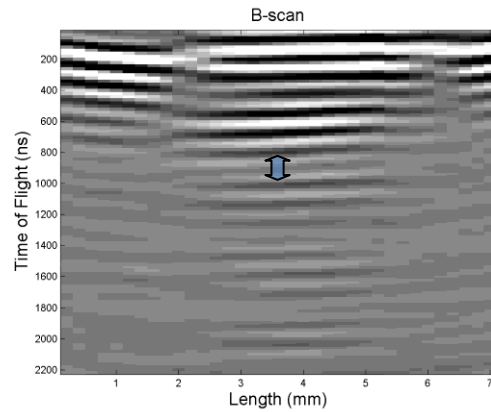
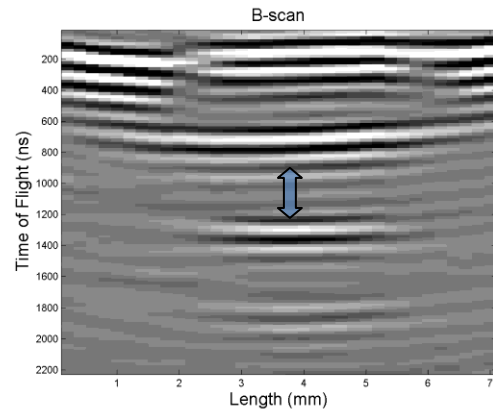


**Figure 4.3.1. Schematic of weld geometry (top) vs. acquired B-scan (bottom).**

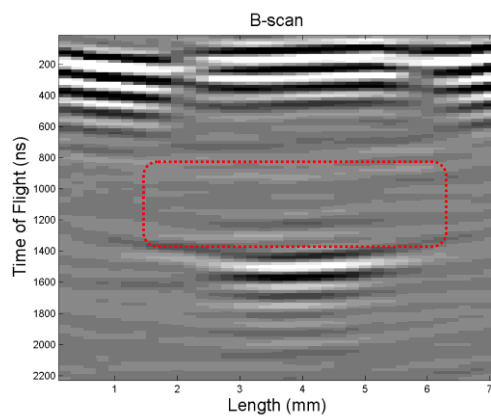
The B-scans acquired could be combined to create a video which provides a cross-sectional view of the welding process. Since a video cannot be placed inside a written document, key frames and images of the video / welding process have been presented. The key frames of the welding process are expected to be similar to stages highlighted in the schematics of Figure 2.1.1. B-scans acquired at 6 different stages during the welding process of a single weld are shown in Figure 4.3.2. The spot weld in this figure was a part of set 2 and was welded at 9.5 kA and labeled weld 9.5kA-a.



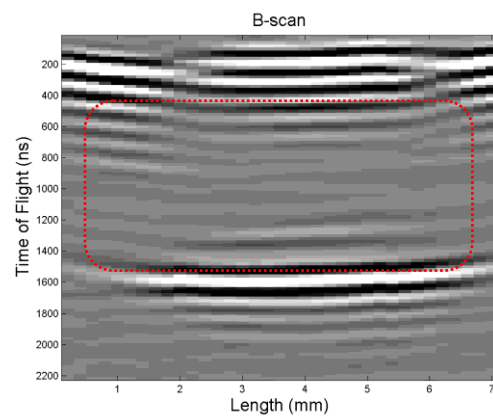
**Closed Jaws**



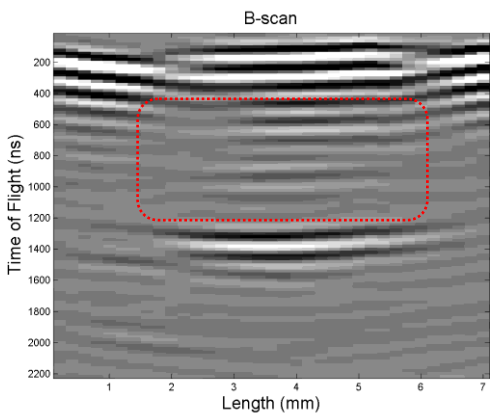
**Just Before Melting**



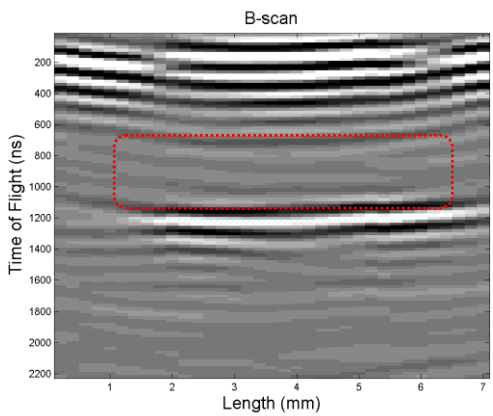
**Nugget Growth**



**Current OFF / Cooling**



**Near Solidification**



**Solidification**

**Figure 4.3.2. B-scans of several spot welding stages.**

It can be observed that in the initial stage when the jaws are closed, the interfaces are closer together. Once the plates were heated the interfaces move apart, caused by the

decrease in speed of sound at higher temperatures. Once the steel is heated enough, it begins to melt at the steel-steel interface and the liquid nugget continues to grow until current is no longer supplied. When current is turned off, the liquid nugget has reached its maximum size and begins to cool and solidify. Eventually the liquid nugget is cooled enough to be fully solidified and a steel-steel interface is no longer present in the B-scan.

In some cases after solidification, the B-scan still shows a reflection between the upper and lower interfaces even for appropriately sized welds. This is due to voids inside the spot weld. A single element transducer would only be able to detect a void if it is directly in the center of the spot weld. The linear phased array transducer improves slightly upon the single element transducer but can only detect voids through a single cross-section of the weld. Figure 4.3.3. shows a B-scan of a completed weld with a reflection between the upper and lower interfaces suggesting a void is present. A cross-section of this weld reveals a void was indeed present near the center of the weld.

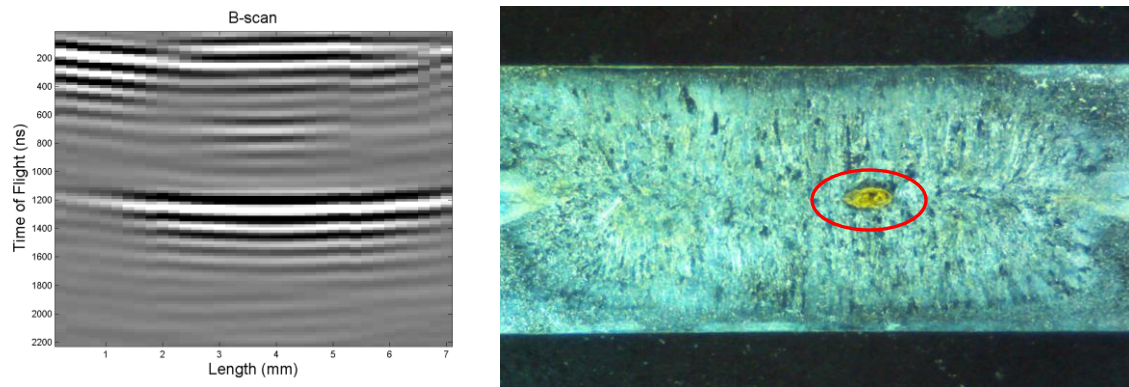


**Figure 4.3.3. Weld 10kA-a B-scan (left) with cross-section (right).**

The A-scans could also be combined to form M-scans of the welding process. Each weld contained an M-scan for every line, meaning 35 M-scans in this experiment. The M-scan of the center line in the linear phased array system is able to acquire an image similar to the M-scans acquired by the existing single element system. Figure

4.3.4. shows a comparison between an M-scan acquired with the existing in-line system and an M-scan from line 18 (center), acquired with the linear phased array system. The key features such as the front-wall, intermediate interface, back-wall, melting point, solidification point, current on position, and total time of flight are still visible using the new system.

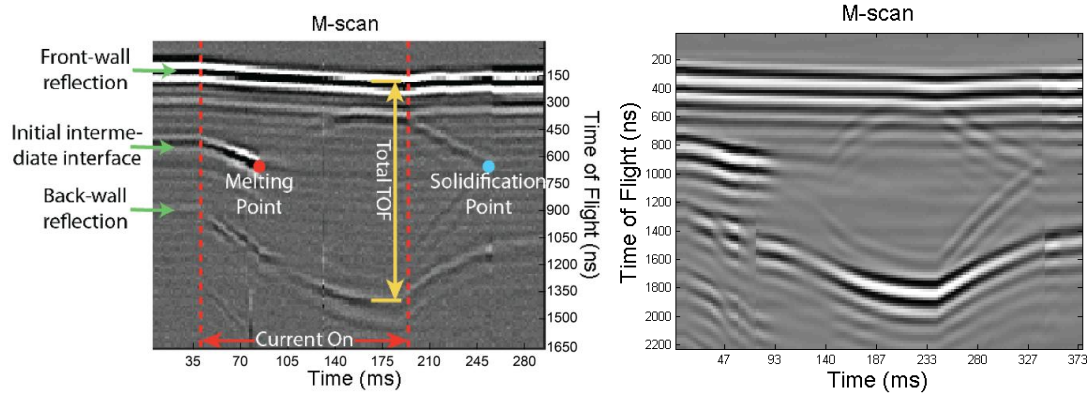


**Figure 4.3.4. Single element M-scan (left) and linear phased array M-scan (right).**

Although the B-scans acquired of the welding process were able to produce nice images, capturing the different stages of the welding process, it was difficult to actually measure nugget sizes from the B-scans. In the B-scans, the upper and lower interface of the liquid nugget was quite clear but it was difficult to see the boundaries of the nugget needed to help determine the nugget diameter. Instead of using B-scans, a method using M-scans was developed to measure the nugget diameter of a weld.

The method for nugget measurement analyzes all 35 M-scans acquired in the welding process. Each M-scan represents a different line through the weld. In each M-scan, the algorithm searches for the presence of a liquid nugget and if it is found, the interface is highlighted. In some M-scans, a faint nugget may appear even when a nugget is not present at that specific location. This was due to the beam width in steel being larger than initially expected caused to the refraction in copper and steel. The beam width

was determined to be larger in steel and greater than the initial 1 mm beam width in water. In order for the algorithm to not consider these faint nuggets, a calibrated threshold was used to determine if the nugget was actually present in the imaged line.

Before searching for the liquid nugget, some image process techniques similar to the ones used in [20] were used to enhance the nugget in the images. First the derivative in the x-direction of the image was taken to detect any changes along the x-direction. Since the nugget growth and solidification appears as diagonal lines the derivative along the x-direction will enhance these diagonal lines. Figure 4.3.5. shows the original M-scan and the M-scan after the derivative along the x-direction has been taken. To detect the liquid nugget, the Hough transform was used to detect lines which make up the nugget. It was noticed that the bottom interface of the liquid nugget during cooling was the strongest reflection of the nugget.

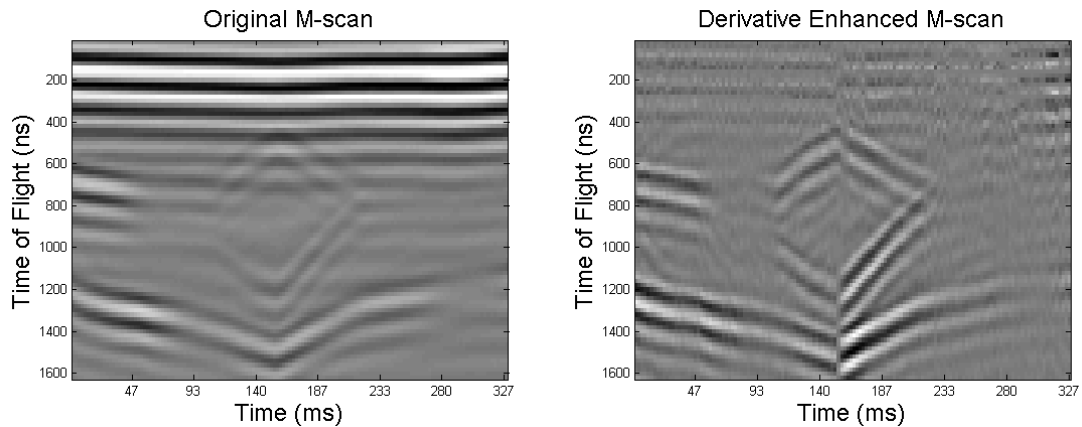


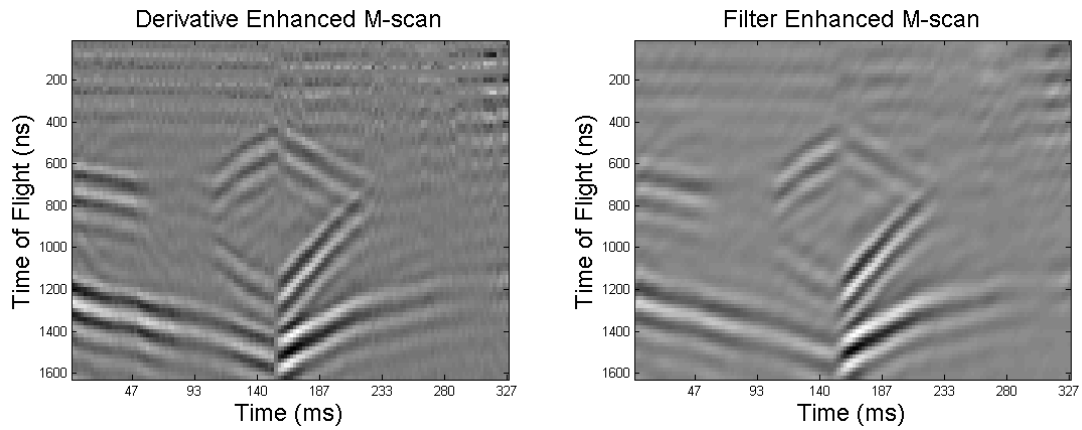
**Figure 4.3.5. Original M-scan (left) &. derivative enhanced M-scan (right).**

Another step was applied to enhance this interface which would be used to determine the presence of the liquid nugget. A filter which enhances diagonal lines with a positive slope was used. This filter is shown in Eqn. 4.3.1.

(Eqn. 4.3.1.)

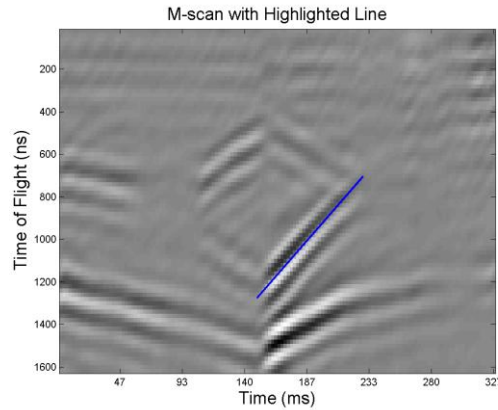
$$\begin{bmatrix} 1 & 1 & 1 & 2 & 3 \\ 1 & 1 & 3 & 4 & 2 \\ 1 & 3 & 6 & 3 & 1 \\ 2 & 4 & 3 & 1 & 1 \\ 3 & 2 & 1 & 1 & 1 \end{bmatrix}$$

Figure 4.3.6. shows the M-scan before and after the diagonal filter was applied. The filter is able to smooth out the image and also enhance the diagonal reflections with a positive slope.



**Figure 4.3.6. Derivative enhanced M-scan (left) & filter enhanced M-scan (right).**

The Hough transform is then used to detect the strongest line with an angle between  $35^\circ$  and  $55^\circ$ . A threshold was calibrated to distinguish between a liquid nugget and a faint liquid nugget which only appears due to the 3 mm beam width in steel. Figure 4.3.7. shows the detected line on the enhanced M-scan. This was performed on all 35 M-scans acquired during welding. Each M-scan represents a region of approximately 0.2 mm. The total number of M-scans with a line detected is then multiplied by the region width of 0.2 to calculate the nugget diameter. The MATLAB code for calculating the nugget diameter can be found in Appendix B – section B.2.



**Figure 4.3.7. M-scan with highlighted line.**

For the example shown, weld 8.5kA-b from set 2 was used. In this example 18 M-scans had a liquid nugget detected so a nugget diameter of  $(18 * 0.0203 = 3.65 \text{ mm})$  was calculated. This calculation is very close to the 3.79 mm measured in the peel test. Table 4.3.1. shows the calculated nugget diameters from both sets of welds. In these results, nugget diameters smaller than 3.5 mm were unable to be detected. This shouldn't be a major problem in production since a 3.5 mm is usually classified as an undersized weld. However, the algorithm could be adjusted to measure these undersized welds more accurately but will reduce the accuracy of the larger welds. There was more focus on properly measuring welds between 4 mm and 7 mm. The maximum nugget diameter which could be calculated was 7.1 mm so welds larger than 7.1 mm were simply calculated as 7.1 mm welds. In some cases, noisy M-scans were present yielding much smaller calculated nugget diameters. For welds which contained clean M-scans, the calculated sizes were fairly close. The thresholds can be further adjusted to improve the calculations for specific applications.



<b>Weld</b>	<b>Set</b>	<b>Actual size (mm)</b>	<b># of Lines Detect</b>	<b>Calculated size (mm)</b>	<b>Error (mm)</b>
9.5kA-a	1	3.59	16	3.25	0.34
9.5kA-b	1	2.27	0	0	n/a
9.5kA-c	1	2.58	0	0	n/a
10kA-a	1	6.12	29	5.88	-0.24
10kA-b	1	5.55	34	6.90	1.35
10kA-c	1	6.45	22	4.46	-1.99
10.5kA-a	1	6.59	33	6.69	0.11
10.5kA-b	1	6.49	33	6.69	0.20
10.5kA-c	1	7.09	35	7.1	0.01
11kA-a	1	7.56	35	7.1	0.46
11kA-b	1	6.42	26	5.27	-1.15
11kA-c	1	7.36	28	5.68	-1.68
8kA-a	2	3.73	18	3.65	-0.08
8kA-b	2	3.03	0	0	n/a
8kA-c	2	3.52	0	0	n/a
8.5kA-a	2	4.55	20	4.06	-0.49
8.5kA-b	2	3.79	18	3.65	-0.14
8.5kA-c	2	4.16	18	3.65	-0.51
9kA-a	2	6.28	26	5.72	-1.00
9kA-b	2	5.58	31	6.29	0.71
9kA-c	2	6.04	29	5.88	-0.15
9.5kA-a	2	6.45	34	6.90	0.44
9.5kA-b	2	5.76	32	6.49	0.73
9.5kA-c	2	6.54	34	6.90	0.36

**Table 4.3.1. Calculated nugget diameters.**

## CHAPTER 5

### CONCLUSIONS AND RECOMMENDATIONS

#### 5.1. Conclusions

Resistance spot welding has been used for many decades and continues to be heavily used by in the automotive industry. It is important to continue to improve on existing methods for quality evaluation of spot welds as well as develop new ways for evaluating these welds. Destructive testing of resistance spot welds is still common practice for many automakers, but with the advancement in technology and in non-destructive testing methods, the frequency in which destructive testing is required should reduce.

The existing single element in-line system for nondestructive evaluation of resistance spot welds is an advanced cutting edge system with many advantages over off-line evaluation methods. With this technology, every spot weld created can be inspected without needing to remove the part from the production line. It is completely automatic and can provide real-time feedback of a spot weld as it is being welded.

An ultrasonic linear phased array system for real-time imaging of resistance spot welds was a logical extension of the existing single element in-line system which also provided a proof of concept to whether a two-dimensional phased array system would be feasible. An understanding of phased array transducers and beam-steering was important in carrying out this research.

The flexibility and programmability of the ULA-OP device was essential in the resistance spot welding application. Having to image through water, copper, and steel required very specific time delays that needed to be calculated and programmed into the

ULA-OP. The ULA-OP was not a commercial product but was geared towards research and development which needed the user to have some programming knowledge in order to properly configure the ULA-OP. One limitation of the ULA-OP was its sampling frequency of 50 MHz. Although 50 MHz is usually adequate in medical imaging, resistance spot welding often involves very thin metal sheets. This made it very difficult to inspect steel plates that were too thin. In the experiments performed, 1.4 mm thickness plates were used in order to be properly imaged. In future generations of the ULA-OP, the sampling frequency will be increased which will eliminate this limitation.

The transducer housing designed was able to protect the transducer from receiving damage from the high electrical current flow in the spot welding process. It was also noticed that there was a slight misalignment of the probe when it was installed inside the housing. This misalignment was due to the probe not sitting tightly enough inside the housing. Since the water lines in the housing were tapped directly through the electrode and into the water channel directly above the transducer, it was very easy for air bubbles to get trapped inside the electrode cap when the system is first turned on. This required the electrode cap to be removed, filled with water and then quickly placed back into place before air could enter the inside of the cap.

The preliminary images acquired of the slots were able to measure slot sizes using some image processing methods. This technique was accurate to  $\pm 0.29$  mm for 5 out of the 7 slot sizes. The different slot sizes helped simulate different sized welds.

The ultrasonic linear phased array system was successful in imaging the entire welding process in real-time. In order to verify what was being imaged by the linear phased array over the welding process, other methods were used to analyze the spot weld

after it was complete. These other methods include off-line acoustic imaging, peel tests, and cross-sections which helped confirm nugget diameters and detect voids within the spot welds. The linear phased array system is able to detect voids within spot weld but is limited to only detecting voids along the path the linear phased array can image. Although the B-scans acquired of the welding process were able to produce a nice video of the welding process, it was difficult to determine an actual nugget diameter from these images. Instead, the M-scans were analyzed to measure nugget diameters. The algorithm for measuring nugget diameter presented provided fairly accurate measurements for welds which did not contain too much noise. The thresholds used in the algorithm could be optimized for specific applications. Finally, it appears likely that the linear phased array system could be successfully extended to a two-dimensional matrix system that could in theory, image the entire region of a spot weld in real-time.

## 5.2.Recommendations

The placement of the water lines inside the welding electrode for the water channel above the transducer made it very easy for air bubbles to be trapped inside the water channel when the system was first turned on. A possible solution would be to install the transducer on the upper jaw instead of the lower jaw. However, for unknown reasons, there is more noise present in the acquisitions when using the upper jaw. The sleeve which held the transducer inside the housing should increase in size slightly, or have another o-ring installed onto it to ensure the probe is aligned properly inside the housing.

To focus the beam along the elevation of the linear phased array, it is recommended to attach a concave acoustic lens to the surface of the transducer. If other

linear phased arrays are to be produced, most transducer manufactures will build a probe with an acoustic lens already attached if requested. Another recommendation would be to use either a concave or convex lens on the electrode cap to generate lines which are perpendicular to the steel plates. This should improve the amplitude of the received signals. The transmission and reception delays could be calculated by modifying the MATLAB code found in Appendix A – section A.1. The inner radius of curvature of the cap would need to be programmed into the weld geometry in the MATLAB script.

If a two-dimensional phased array is to be use, a lens attached to the transducer would no longer be needed or useful. There are many resources available that investigate optimal transducer design which should be referred to while designing a phased array for the welding application. A concave welding electrode cap in this case could also possibly improve the beam width. The use of a two-dimensional linear phased array system could prove to be the next big advancement in in-line non-destructive evaluation of resistance spot welds.

## REFERENCES

- [1] H. Zhang and J. Senkara, "Resistance Welding: Fundamentals and Applications," CRC Press; 1st edition, 2005.
- [2] "Snell's law." Wikipedia: The Free Encyclopedia. Wikimedia Foundation, Inc. 12 July 2012. Web 29 July. 2012.
- [3] M. A. Al-Jader, N. Wylie, J. D. Cullen, A.I. Al-Shamma'a, "Investigation Into Spot Welding Process Sustainability For the Automotive Industry," 5<sup>th</sup> Annual BEAN Conference LJMU, 2010.
- [4] Y. J. Chao, "Ultimate Strength and Failure Mechanism of Resistance Spot Weld Subjected to Tensile, Shear, or Combined Tensile/Shear Loads," Journal of Engineering Materials and Technology, vol. 125, 2003.
- [5] B.W. Drinkwater and P. D. Wilcox, "Ultrasonic arrays for non-destructive evaluation: A review," Nondestructive Testing and Evaluation International 39, 2006.
- [6] K. J. Kirk, A. McNab, A. Cochran, I. Hall, G. Hayward, "Ultrasonic Arrays for Monitoring Cracks in an Industrial Plant at High Temperatures," IEEE Transactions on Ultrasonics, Ferroelectrics, and Frequency Control, vol. 46, no. 2, 1999.
- [7] S. J. Song, H. J. Shin, Y. H. Jang, "Development of an ultrasonic phased array system for nondestructive tests of nuclear power plant components," Nuclear Engineering and Design 214, 2002.
- [8] S. Chatillon, G. Cattiaux, M. Serre, O. Roy, "Ultrasonic non-destructive testing of pieces of complex geometry with a flexible phased array transducer," Ultrasonics 38, 2000.
- [9] R. Gr. Maev, et al., "Method and apparatus for assessing quality of spot welds," US Patent Number 7,775,415, Filed: June 14, 2005, Issued: August 17, 2010.
- [10] A. M. Chertov and R. Gr. Maev, "Determination of resistance spot weld quality in real time using reflected acoustic waves. Comparison with through-transmission mode," 16<sup>th</sup> World Conference on Nondestructive Testing, Montreal, Quebec, September 2004.
- [11] R. Gr. Maev, A. Ptchelintsev, J. Mann, "Transducer built into an electrode," US Patent Number 6,297,467, Filed: April 1, 1999, Issued: October 2, 2001.
- [12] A. M. Chertov, et al., "In-process ultrasound NDE of resistance spot welds," The British Institute of Non-Destructive Testing Insight, vol. 54, no. 5, 2012

- [13] "Snell's law." Wikipedia: The Free Encyclopedia. Wikimedia Foundation, Inc. 23 July 2012. Web 01 Aug. 2012.
- [14] S. C. Wooh and Y. Shi, "A Simulation Study of Beam Steering Characteristics for Linear Phased Arrays," *Journal of Nondestructive Evaluation*, vol. 18, no. 2, 1999.7
- [15] S. C. Wooh and Y. Shi, "Optimization of Ultrasonic Phased Arrays," *Review of Progress in Quantitative Nondestructive Evaluation*, eds., D.O. Thompson and D.E. Chimenti, vol. 17, Plenum Press, New York., 1998.
- [16] P. Tortoli, et al., "ULA-OP: An advanced open platform for ultrasound research," *IEEE Trans. on UFFC*, vol. 56, no. 10, 2009.
- [17] MSDLab, ULA-OP Manual ver. 1.5.1., Firenze, February 2012.
- [18] B. P. Lathi, "Linear Systems and Signals," 2<sup>nd</sup> Edition, Oxford University Press, Inc., 2005 (pp. 363-364, 770-773).
- [19] Weisstein, Eric W. "Least Squares Fitting." From MathWorld – A Wolfram Web Resource. <http://mathworld.wolfram.com/LeastSquaresFitting.html>.
- [20] A.C. Karloff, A.M. Chertov, R. Gr. Maev, "Enhancing Real-time Ultrasound Signatures of Molten Nugget Growth for Quality Evaluation of Resistance Spot Welds," *IEEE Ultrasonics Symposium*, Sept. 2009.

## APPENDICES

### APPENDIX A

#### ULA-OP Files & Code

##### A.1. Calculating Transmission and Reception Delays

```
go_run_rx = 0;
go_run_tx = 1;

%% Probe
NElements = 24; % - Number of Elements on the probe
ElementPitch = .2; % [mm] - Element pitch of the probe

%% Lines
NLines = 35; % - Number of lines per (b-mode) frame
MaxAngle = 6.5; % [°] - Angle of the most steered line inside copper
MaxX = 3.5; % [mm] - X pass point of the most steered line (from
center of probe)
MaxDZ = 12; % [mm] - Z psas point of the most steered line (from
water-copper layer)

%% Media
WaterDZ = 20; % [mm] - Probe to water-copper interface distance
(water thickness)
CopperDZ = 12; % [mm] - Copper thickness
WaterC = 1480e3; % [mm/s] - Speed of sound inside Water
CopperC = 4660e3; % [mm/s] - Speed of sound inside Copper
CopperWindowX = 4; % [mm] - Copper surface window (one side, used only
for matlab display)

%% Focusing & System
StartZ = 14; % [mm] - Minimum depth for dynamic (RX) focusing,
along vertical line (must be inside water)
EndZ = 42; % [mm] - Maximum depth for dynamic (RX) focusing,
along vertical line (must be beyond water-copper interface)
TxFocusZ = 32.5; % [mm] - Focusing depth for transmission (TX),
along vertical line (must be beyond water-copper interface)
RxSamplingFreq = 50e6; % [Hz] - RX sampling frequency
TxSamplingFreq = 600e6; % [Hz] - TX sampling frequency
TxFrequency = 10e6; % [Hz] - TX burst frequency
TxCycles = 1; % - Number of cycles of TX burst (can be multiple
of 0.5)
SpecialTx = 1; % - Applies special TX burst (1.5 cycles balanced
burst with thinner edges _--_)
ApodizationType = 1; % - Applies apodization to both TX and RX
% - 0 = None, 1 = Symmetric on edges, 2 = Fixed

%% --- Format Probe -----
ne2 = NElements/2-.5;
```



```

ElementX = ElementPitch * (-ne2:1:ne2);

%% --- Get RX Lines -----
MaxAngle1 = asind(WaterC/CopperC*sind(MaxAngle));
IntX2 = MaxX-MaxDZ*tand(MaxAngle);

RotPointX1 = 0;
RotPointZ1 = WaterDZ - IntX2/tand(MaxAngle1);
AngleStep1 = 2*MaxAngle1/(NLines-1);
Angles1 = -MaxAngle1:AngleStep1:MaxAngle1;

db = WaterC / (2*RxSamplingFreq);
mind = StartZ-RotPointZ1;
for k = 1:NLines
    maxd = (WaterDZ-RotPointZ1)/cosd(Angles1(k));
    d = mind:db:maxd;
    LinesZ1{k} = d*cosd(Angles1(k))+RotPointZ1;
    LinesX1{k} = d*sind(Angles1(k))+RotPointX1;
end

Angles2 = asind(CopperC/WaterC*sind(Angles1));
IntsX2 = (WaterDZ-RotPointZ1)*tand(Angles1);

db = CopperC / (2*RxSamplingFreq);
for k = 1:NLines
    remd = sqrt((LinesZ1{k}(end)-WaterDZ).^2 + (LinesX1{k}(end)-
IntsX2(k)).^2);
    mind = db-remd;
    maxd = EndZ-WaterDZ;
    d = mind:db:maxd;
    LinesZ2{k} = d*cosd(Angles2(k)) + WaterDZ;
    LinesX2{k} = d*sind(Angles2(k)) + IntsX2(k);
end

m = floor((NLines+1)/2);
ntot = length(LinesZ1{m}) + length(LinesZ2{m});

for k = 1:NLines
    n = length(LinesZ1{k});
    LinesZ2{k} = LinesZ2{k}(1:ntot-n);
    LinesX2{k} = LinesX2{k}(1:ntot-n);
end

%% --- Get TX Points -----
if(TxFocusZ < WaterDZ)
    error('err');
end

d = TxFocusZ-RotPointZ1 - (WaterDZ-RotPointZ1)./cosd(Angles1);
PointsZ1 = d.*cosd(Angles2) + WaterDZ;
PointsX1 = d.*sind(Angles2) + IntsX2;

%% --- RX Delays -----
IntsX1 = -RotPointZ1*tand(Angles1);
vratio = WaterC/CopperC;

```

```

if go_run_rx

    for k = 1:NLines
        l = length(LinesZ1{k});
        ex = repmat(ElementX, [l 1]);
        lz = repmat(LinesZ1{k}', [1 NElements]);
        lx = repmat(LinesX1{k}', [1 NElements]);
        Delays{k} = sqrt( (lx-ex).^2 + lz.^2 ) / WaterC;
    end

    l = length(LinesZ2);
    ma = MaxAngle+2;
    t2 = tand( -ma:.1:ma );
    wzt1 = WaterDZ*tand( asin( WaterC/CopperC*sind(t2) ) );
    ex = repmat(ElementX, [length(t2) 1]);
    t2 = repmat(t2', [1 NElements]);
    wzt1 = repmat(wzt1, [1 NElements]);

    % Delays in Copper

    for k = 1:NLines
        waitbar(k/NLines);
        l2 = length(LinesZ2{k});
        ex2 = repmat(ElementX, [l2 1]);
        lz2 = repmat(LinesZ2{k}', [1 NElements]);
        lx2 = repmat(LinesX2{k}', [1 NElements]);
        copperzdim = lz2 - 20;
        calcx = ex2 - lx2;

        % determine angles
        for i = 1:l2
            for j = 1:NElements
                maxA = 18;
                minA = -18;
                while 1
                    avg = (maxA+minA)/2;
                    test = WaterDZ*tand(avg) + copperzdim(i,j)*
                        tand(asind(sind(avg)/vratio));
                    if abs(test - calcx(i,j)) < 0.0001
                        theta1(i,j) = abs(avg);
                        break;
                    elseif test > calcx(i,j)
                        maxA = avg;
                    elseif test < calcx(i,j)
                        minA = avg;
                    end
                end
            end
        end
        Theta1{k} = theta1;
        clear theta1;
        Theta2{k} = asind(sind(Theta1{k})./vratio);
        Delays2{k} = (20./cosd(Theta1{k}))./WaterC +
            (copperzdim./cosd(Theta2{k}))./CopperC;
    end
end

```

```

% Combine Delays
for i = 1:NLines
    Delay_All{i} = [Delays{i};Delays2{i}];
end

if(StartZ > WaterDZ)
    error('err');
end

d = 0:size(Delay_All{k}, 1)-1;
d = d / RxSamplingFreq / 2;
d = d + StartZ/WaterC;
d = repmat(d', [1 NElements]);
for k = 1:NLines
    Delay_All{k} = Delay_All{k} + d;
end

close( waitbar(1) );

end % go_run_rx

%% --- TX Delays -----
if go_run_tx

    ex = repmat(ElementX, [NLines 1]);
    lz = repmat(PointsZ1', [1 NElements]);
    lx = repmat(PointsX1', [1 NElements]);
    lp = length(PointsZ1);
    calcx = ex-lx;
    copperzdim = lz - 20;
    for i = 1:lp
        for j = 1:NElements
            maxA = 18;
            minA = -18;
            while 1
                avg = (maxA+minA)/2;
                test = WaterDZ*tand(avg) +
copperzdim(i,j)*tand(asind(sind(avg)/vratio));
                if abs(test - calcx(i,j)) < 0.0001
                    theta1(i,j) = abs(avg);
                    break;
                elseif test > calcx(i,j)
                    maxA = avg;
                elseif test < calcx(i,j)
                    minA = avg;
                end
            end
        end
    end

    theta2 = asind(sind(theta1)./vratio);
    TxDelays = (20./cosd(theta1))./WaterC +
(copperzdim./cosd(theta2))./CopperC;

    TxDelays = -TxDelays;

```

```

for k = 1:NLines
    d = abs(ElementX-IntsX1(k));
    ii1 = find(d == min(d), 1);
    d = [d(1:ii1-1) d(ii1+1:end)];
    ii2 = find(d == min(d), 1);

    if(ii2 == ii1)
        ii1 = ii1+1; % ii2 = ii1+1; swap ii2, ii1
    end
    rd = TxDelays(k,ii2) + (IntsX1(k)-ElementX(ii2)) *
((TxDelays(k,ii1)-TxDelays(k,ii2))/ElementPitch);
    TxDelays(k,:) = TxDelays(k,:) - rd;
end

mm = min(min(TxDelays));
BurstFactor = abs(mm);

TxDelays = TxDelays - mm;

end % go_run_tx

%% --- TX Signal -----
TxSignal = [];
t1 = round(TxSamplingFreq/TxFrequency/2);
t2 = round(TxSamplingFreq/TxFrequency) - t1;

if(SpecialTx)

    t3 = round(TxSamplingFreq/TxFrequency/4);
    TxSignal = [-ones(1,t3) ones(1,t1) -ones(1,t3)];

    if(exist('BurstFactor', 'var'))
        BurstFactor = BurstFactor + 1/TxFrequency/2;
    end

else

    for k = 1:floor(TxCycles)
        TxSignal = [TxSignal ones(1,t1) -ones(1,t2)];
    end

    if((TxCycles-k) ~= 0)
        TxSignal = [TxSignal ones(1,t1)]; %% Half cycle only
    end

    if(exist('BurstFactor', 'var'))
        BurstFactor = BurstFactor + TxCycles/TxFrequency/2;
    end

end

TxSignal = [0 TxSignal 0];

```

```

%% --- Active elements -----
if(ApodizationType == 0)
    %% All elements active
    ActiveElements = ones(NLines, NElements);
end
if(ApodizationType == 1)
    %% Symmetric aperture
    ActiveElements = zeros(NLines, NElements);
    for k=1:NLines
        n = round(Intsx1(k)/.2);
        p1 = max(1, n+1);
        p2 = min(NElements, NElements+n);
        ActiveElements(k,p1:p2) = 1;
    end
end
if(ApodizationType == 2)
    %% Fixed aperture
    ActiveElements = zeros(NLines, NElements);
    mn = abs(round(Intsx1(1)/.2)) ;
    for k=1:NLines
        n = round(Intsx1(k)/.2);
        p1 = n+mn+1;
        p2 = NElements-mn+n;
        ActiveElements(k, p1:p2) = 1;
    end
end

%% --- Graph -----
figure(1); clf;

hold on
plot([ElementX(1) ElementX(end)], -[0 0], 'g');
plot([-CopperWindowX CopperWindowX], -[WaterDZ WaterDZ], 'b');
plot([-CopperWindowX CopperWindowX], -(CopperDZ+[WaterDZ WaterDZ]),
'b');

for k = 1:NLines
    plot(LinesX2{k}, -LinesZ2{k}, 'r');
end

for k = 1:NLines
    plot(LinesX1{k}, -LinesZ1{k}, 'k');
end

plot(PointsX1, -PointsZ1, 'ro');
hold off;

%% --- ULA ---
fprintf('\nFrom Water\n');
fprintf('Nlines = %d\n', NLines);
fprintf('ScanStep = %.2f\n', AngleStep1);
fprintf('YPhasing = %.2f\n', RotPointZ1);
fprintf('RxPass = %.2f\n', Intsx2(1));
fprintf('RyPass = %.2f\n', WaterDZ);
fprintf('RxAngle = %.2f\n', -MaxAngle1);
fprintf('RyMin = %.2f\n', StartZ);

```

```

fprintf('RyMax = %.2f\n', EndZ);

fprintf('\nFrom Copper\n');
fprintf('Nlines = %d\n', NLines);
fprintf('ScanStep = %.2f\n', Angles2(2)-Angles2(1));
fprintf('YPhasing = %.2f\n', WaterDZ-(MaxX/tand(MaxAngle) - MaxDZ));
fprintf('RxPass = %.2f\n', IntsX2(1));
fprintf('RyPass = %.2f\n', WaterDZ);
fprintf('RxAngle = %.2f\n', -MaxAngle);
fprintf('RyMin = %.2f\n', StartZ);
fprintf('RyMax = %.2f\n', EndZ);

```

## A.2. Generating bft Files for Transmission

```

filename = 'inline35lines_apod.bfr';

fid = fopen(filename, 'wb');

N = length(Delay_All)*NElements; % # of Delay waveforms
J = 2; % # of Apodization waveforms
M = length(Delay_All{1}); % # of delays/apod samples in waveforms
ds = 1; % downsampling factor
K = NElements; % # of probe elements
F = NLines; % # of lines

fwrite(fid, [N J M ds K F], 'uint16');

for i = 1:NLines
    fwrite(fid, Delay_All{i}, 'float32');
end

fwrite(fid, zeros(1, M), 'float32'); % standard apod waveform
fwrite(fid, ones(1, M), 'float32'); % null apod waveform (when
element should be disabled)

for j=1:F
    for k = 1:K
        fwrite(fid, k-1, 'uint16');
        fwrite(fid, (j-1)*K+k, 'uint16');
        fwrite(fid, ActiveElements(j, k)+1, 'uint16');
    end
end

fclose(fid);

```

## A.3. Generating bfr Files for Reception

```

filename = 'inline35lines_apod.bfr';

fid = fopen(filename, 'wb');

N = length(Delay_All)*NElements; % # of Delay waveforms

```

```

J = 2; % # of Apodization waveforms
M = length(Delay_All{1}); % # of delays/apod samples in waveforms
ds = 1; % downsampling factor
K = NElements; % # of probe elements
F = NLines; % # of lines

fwrite(fid, [N J M ds K F], 'uint16');

for i = 1:NLines
    fwrite(fid, Delay_All{i}, 'float32');
end

fwrite(fid, zeros(1, M), 'float32'); % standard apod waveform
fwrite(fid, ones(1, M), 'float32'); % null apod waveform (when
element should be disabled)

for j=1:F
    for k = 1:K
        fwrite(fid, k-1, 'uint16');
        fwrite(fid, (j-1)*K+k, 'uint16');
        fwrite(fid, ActiveElements(j, k)+1, 'uint16');
    end
end

fclose(fid);

```

#### A.4.ULA-OP Configuration File (.cfg)

```

[NAME] // Scan Name - main screen
Name = Phasing Water+Copper (W)

[COMMENT] // Scan Comment - side screen
Comment = 35 Lines, 24 element Single Scan

[TREE] // window setup
aspect = 1H0
ratio = 100

[WORKINGSET]
SoundSpeed = 1480 // sound speed for focusing

//[SAVEOPT]
//Auto = ,,9600

[SSG]
PrfsMap = 2000, 4000, 6250, 8000, 10000, 12000, 13000, 14000, 15000, 16000, 17000,
18000, 19000, 20000
PRF = 15000 // default pulse rep. freq (Hz) - speed of

```

```

[SEQUENCER]                                // various imaging / array scanning sequences - each
item// line is a different imaging rule
item0 = manual.ula

                                           // define imaging rules (scan type, focusing, frequencies)
                                           // YOU CAN'T PUT A COMMENT ON THAT LINE!! ->

FILE ERROR

[ACQUIREIQ]                               // define //d image data slices
slice0 = nGates 256, nPRI 12500, StartGate 0, SliceIQ, 1, NoSave

// 2nd slice would go here if needed - so modules can use independant data

[ACQUIRERF]
rftype = Post                             // RF type 0=None (?), 1 = Pre-BF, 2
= Post then some loss/attenuation of RF signal
BfLoss = 3                               // another loss/attenuation of
signal

[ACQUIRERF_Post]
slice0 = 512, 12500, 800, SliceRF, 1, Save    // Use this for welds
//slice0 = 512, 350, 800, SliceRF, 1, Save    // Use this for slots
RfLoss = 3

[BLOCKSEQUENCER]                           // how the slices are sequenced, and when rx/tx
rules change
pri0 = item 0, count 1, sliceiq 0, merge 0, slicerf 0

// 2nd pri goes here, grabs another slice of data
// can have modules (below) use 2 independant data to create image so they aren't
"hooked" in time

[MODULES]                                  // define various modules to use, names arbitrary, link to modules
below
module0 = Bmodel1
[Bmodel1]                                  // Image1 corresponds to module name. CModBMode = BScan
module
ModuleName = CModBMode
SizeX = 35                                // image / window size
SizeY = 256
Window = 0                                // put image in this window
Slice = 0                                  // use this slide data
Threshold = 18                             // display threshold [don't display below //]
Dynamic = 4                                // gray scale map gradient - lower = brighter faster, higher = brigrter
slower

```



```
VideoFilter = 1           // video display rate - higher = more visual display
averaging (less flutter)
ViewItem = 0             // A special reference number
RatioBase = 210
```

#### A.5.ULA-OP ULA File (.ula)

```
[GLOBAL]
Name = Manual
Nlines = 35
ScanType = 1
ScanStep = .12
YPhasing = -39.28
LineOffset = 0

[TXSETTINGS]
TxFromFile = 1
TxFileName = inline35lines.bft
TxAmp = 1.3
```

```
[RXSETTINGS]
RxFromFile = 1
RxFileName = inline35lines.bfr
RxAngle = -2.06
RXPass = -2.13
RYPass = 20
RYMax = 42
RYMin = 14
```

```
[RXANALOG]
Tgc = 0, 11
```

```
[RXELAB]
DemodulationFrequency = 10000000
Ncpm = 4, 5, 5, 6           // filters that we leave
                               // at these numbers
NDec = 1, 1, 2              // the last changes sampling rate 1=50, 2=25, 3=50/3
                               // same as fburst in [i] tool
```

## APPENDIX B

### Image Processing MATLAB Code

#### B.1. Slot Size Measurement

```
%% MATLAB script for calculating slot sizes
DefaultDir = 'C:\Documents and Settings\My Documents\Thesis\
slotmeasure';
BFRfile = 'C:\Documents and Settings\My Documents\Thesis\
slotmeasure\inline35lines_apod.bfr';
%%
NLinesPerFrame = 35;
%%
Speed = 5700e3; % [mm/s]
SmpFreq = 50e6; % [Hz]
TxFreq = 10e6; % [Hz]

%% --- GetFile -----
[FileName,PathName] = uigetfile({'*.rfb','RF post file
(*.rfb)'},'Please select a post-beamforming data file', DefaultDir);
if (FileName==0)
    return;
end
[mat, NFrames] = loadpost(FileName, PathName, NLinesPerFrame);
NGates = size(mat,1);
mat = reshape(mat, [NGates NLinesPerFrame NFrames]);

%% --- Load BFR file and apply correction (due to ULA-OP FE error) ----
if(1)
    fid = fopen(BFRfile, 'rb');
    if (fid==-1)
        return;
    end
    a = fread(fid, 6, 'uint16');
    DelayWaveforms = fread(fid, [a(3) a(1)], 'float32');
    DelayWaveforms = reshape( DelayWaveforms(1, :), [24
        NLinesPerFrame]);
    fseek(fid, a(3)*a(2)*4, 0);
    e = fread(fid, 3*a(5)*a(6), 'uint16');
    e = reshape(e, [3 a(5) a(6)]);
    e = squeeze(e(3,:,:));
    m = ones(NLinesPerFrame, 1);
    if(1)
        m = sum(e).^2;
    end
    fclose(fid);
    MaxC = max(e .* DelayWaveforms);
    StrC = round(MaxC*SmpFreq);
    StrC = StrC-min(StrC);
    l = size(mat,1);
    for k=1:NLinesPerFrame
        c = StrC(k);
        mat(1:(l-c),k,:) = mat((c+1):l,k,:);
    end
end
```

```

    mat(:, k, :) = mat(:, k, :) / m(k);
end
end

%% --- Demodulation -----
n = 1:NGates;
Demodulated = mat .* repmat(exp(1i*2*pi*TxFreq*n'/SmpFreq), [1
NLinesPerFrame NFrames]);
taps = firpm(32, [0 .05 .3 1], [1 1 0 0], [1 1]);
Demodulated = filter(taps, 1, [Demodulated ; zeros([16 NLinesPerFrame
NFrames])]);
Demodulated = Demodulated(17:end,:,:)

%% --- Window ----
mat = mat(230:310, :, 1);
Demodulated = Demodulated(230:310, :, 1);
Preinterp = Demodulated;
Demodulated = interp2(Demodulated, 1:.25:35,
(1:.5:size(Demodulated,1))', 'cubic');
Amp = abs(Demodulated);
figure(1);
colormap gray;
imagesc(mat);
xlabel('Length (mm)', 'FontSize', 18), ylabel('Time of Flight
(ns)', 'FontSize', 18), title('B-scan - 5 mm Slot', 'FontSize', 20),
oldylabels=get(gca, 'ytick');
newylabels=oldylabels*20;
set(gca, 'yticklabel', newylabels, 'FontSize', 14);
newxticks = [3.3 8.2 13.1 18 22.9 27.8 32.7];
newxlabel=[-3 -2 -1 0 1 2 3];
set(gca, 'xtickmode',
'manual', 'xtick', newxticks, 'xticklabel', newxlabel, 'FontSize', 14);

figure(2);
colormap gray;
imagesc(Amp);
xlabel('Length (mm)', 'FontSize', 18), ylabel('Time of Flight
(ns)', 'FontSize', 18), title('B-scan - 5 mm Slot', 'FontSize', 20),
oldylabels=get(gca, 'ytick');
newylabels=oldylabels*10;
set(gca, 'yticklabel', newylabels, 'FontSize', 14);
newxticks = [11.4 30.6 49.8 69 88.2 107.4 126.6];
newxlabel=[-3 -2 -1 0 1 2 3];
set(gca, 'xtickmode',
'manual', 'xtick', newxticks, 'xticklabel', newxlabel, 'FontSize', 14);

%% --- measure ----
[gx, gy, button] = ginput(1);
if( isempty(gx) || (button~=1) )
    return;
end
ext = max(Amp(round(gy-10):round(gy+10), :), [], 1);
figure(2);
hold on;
rectangle('Position', [1, gy-10, 136, 21], 'EdgeColor', 'r');

```

```

hold off;
figure(3);
plot( ext );
xlabel('Length (mm)', 'FontSize', 18), ylabel('Relative
Amplitude', 'FontSize', 18), title('Amplitude Plot - 5 mm
Slot', 'FontSize', 20), % in Time',
oldylabels=get(gca, 'ytick');
newylabels=oldylabels;
set(gca, 'yticklabel', newylabels, 'FontSize', 14);
newxticks = [11.4 30.6 49.8 69 88.2 107.4 126.6];
newxlabels=[-3 -2 -1 0 1 2 3];
set(gca, 'xtickmode',
'manual', 'xtick', newxticks, 'xticklabel', newxlabels, 'FontSize', 14);

%%%%%%%%
mx = max(ext);
ii = find(ext > (mx*.9)); %Find indexes where ext > mx * .9
a = mean(ext(ii)) / 1; % .99
m = 0;
sma = 17;
x = -37:-1;
gs1 = a*exp(-.5*((x-m).^2)/sma^2);
l = length(gs1);
l2 = l/2-.5;

% left side
errs = zeros(1, 100);

% Fit with least mean square error
for k=1:100
    i1 = max(1, k-l2);
    i2 = min(137, k+l2);
    sext = ext(i1:i2);
    i1 = max(l2-k+2, 1);
    i2 = min(137-l2+l-k, 1);
    sgs = gs1(i1:i2);
    errs(k) = sum((sgs-sext).^2);
end
[mne, mnei1] = min(errs);
% right side
errs = zeros(1, 137-37+1);
gs2 = fliplr(gs1);
for k=37:137
    i1 = max(1, k-l2);
    i2 = min(137, k+l2);
    sext = ext(i1:i2);
    i1 = max(l2-k+2, 1);
    i2 = min(137-l2+l-k, 1);
    sgs = gs2(i1:i2);
    errs(k-37+1) = sum((sgs-sext).^2);
end
[mne, mnei2] = min(errs);
mnei2 = mnei2 + 37-1;

figure(3);
hold on;

```

```

plot((1:1)-l2-1+mnei1, gs1,'r');
plot((1:1)-l2-1+mnei2, gs2,'r');
hold off;
sp1 = 1.15;
sp2 = 1.4;
rc = sp1:((sp2-sp1)/75):sp2;
sma1 = sma * rc(mnei1);
sma2 = sma * rc(144-mnei2);
i1 = mnei1 -sma1 + (l2+1);
i2 = mnei2 +sma2 - (l2+1);
stp=7.1/length(ext);
fprintf('Pixels - %f\n', abs(i1-i2));
fprintf('Size - %.2f\n', (abs(i1-i2))*stp );
fprintf('\n');

```

## B.2. Weld Nugget Size Measurement

%% MATLAB script for calculating nugget diameter from spot welds  
 %% Note: Hough function used to detect lines in grayscale images was developed by Tao Peng Copyright © 2006 and can be found in the MATLAB file exchange by searching for the developer.

```

% If new scan is to be loaded
if (1)
clear all;
n_lines = 35;
[FileName,PathName] = uigetfile({'*.bin;*.rfb','RF post file (*.bin;*.rfb)'},'Please select a post-beamforming data file');
if FileName~=0
    h = waitbar(1,'Please wait...');
    File=[PathName,FileName];
    [pathstr, name, ext, versn] = fileparts(File);
    if strcmp(ext, '.bin')
        file_info=[PathName name '_info.txt'];
    else
        file_info=[PathName name '.uos'];
    end
    newData1 = importdata(file_info);
    vars = fieldnames(newData1);

    if strcmp(ext, '.bin')
        for i = 1:length(newData1.data)
            assignin('caller',
                    newData1.textdata{i,1},newData1.data(i));
        end
    else
        for i = 2:length(newData1.textdata)
            assignin('caller', newData1.textdata{i,1},newData1.data(i-1));
        end
    end
    fid = fopen(File,'r');
    src = fread(fid,TotalSize,'int16=>int16');
    fclose(fid);

```

```

l = length(src);
fpga = reshape(src, [4 1/4]);
quattro = permute(fpga, [2 1]);
quattro = reshape(quattro, [4 2 1/4/4/2 4]);
clear fpga
ab = permute(quattro, [1 3 2 4]);
ab = reshape(ab, [1/4/2 2 4]);
clear quattro
ppmat = reshape(ab, [1/4/2 8]);
clear ab
ppmat=reshape(ppmat,BlockLength,[],8);

if ~exist('n_lines','var')
    scartati=0;
else
    if mod(FirstBlock,n_lines)==0
        scartati=0;
    else
        scartati=n_lines-mod(FirstBlock,n_lines);
    end
end
ppmat=circshift(ppmat,[0 -scartati 0]);
post_beamforming = sum(ppmat,3);
clear ppmat;
post_beamforming=single(post_beamforming);
close(h);
end

figure(1);
colormap gray;
[l1, l2] = size(post_beamforming);
n_frames = floor(l2/n_lines);
post_beamforming = post_beamforming(:,1:n_frames*n_lines);
mat = reshape(post_beamforming, [l1 n_lines n_frames]);
cut_off = 14;
% Apply image correction Set 1(due to ULA-OP FE error) ----
if (0)
    mat2(:,18,:) = mat(1:end-cut_off,18,:);
    mat2(:,17,:) = mat(2:end-cut_off+1,17,:);
    mat2(:,19,:) = mat(2:end-cut_off+1,19,:);
    mat2(:,16,:) = mat(3:end-cut_off+2,16,:);
    mat2(:,20,:) = mat(3:end-cut_off+2,20,:);
    mat2(:,15,:) = mat(3:end-cut_off+2,15,:);
    mat2(:,21,:) = mat(3:end-cut_off+2,21,:);
    mat2(:,14,:) = mat(4:end-cut_off+3,14,:);
    mat2(:,22,:) = mat(4:end-cut_off+3,22,:);
    mat2(:,13,:) = mat(5:end-cut_off+4,13,:);
    mat2(:,23,:) = mat(5:end-cut_off+4,23,:);
    mat2(:,12,:) = mat(5:end-cut_off+4,12,:);
    mat2(:,24,:) = mat(5:end-cut_off+4,24,:);
    mat2(:,11,:) = mat(6:end-cut_off+5,11,:);
    mat2(:,25,:) = mat(6:end-cut_off+5,25,:);
    mat2(:,10,:) = mat(7:end-cut_off+6,10,:);
    mat2(:,26,:) = mat(7:end-cut_off+6,26,:);
    mat2(:,9,:) = mat(8:end-cut_off+7,9,:);
    mat2(:,27,:) = mat(8:end-cut_off+7,27,:);

```

```

mat2(:,8,:) = mat(9:end-cut_off+8,8,:);
mat2(:,28,:) = mat(9:end-cut_off+8,28,:);
mat2(:,7,:) = mat(9:end-cut_off+8,7,:);
mat2(:,29,:) = mat(9:end-cut_off+8,29,:);
mat2(:,6,:) = mat(10:end-cut_off+9,6,:);
mat2(:,30,:) = mat(10:end-cut_off+9,30,:);
mat2(:,5,:) = mat(10:end-cut_off+9,5,:);
mat2(:,31,:) = mat(10:end-cut_off+9,31,:);
mat2(:,4,:) = mat(11:end-cut_off+10,4,:);
mat2(:,32,:) = mat(11:end-cut_off+10,32,:);
mat2(:,3,:) = mat(11:end-cut_off+10,3,:);
mat2(:,33,:) = mat(11:end-cut_off+10,33,:);
mat2(:,2,:) = mat(12:end-cut_off+11,2,:);
mat2(:,34,:) = mat(12:end-cut_off+11,34,:);
mat2(:,1,:) = mat(12:end-cut_off+11,1,:);
mat2(:,35,:) = mat(12:end-cut_off+11,35,:);
end

% Apply new image correction Set 2(due to ULA-OP FE error) ----
if (1)
    mat2(:,18,:) = mat(1:end-cut_off,18,:);
    mat2(:,17,:) = mat(2:end-cut_off+1,17,:);
    mat2(:,19,:) = mat(2:end-cut_off+1,19,:);
    mat2(:,16,:) = mat(3:end-cut_off+2,16,:);
    mat2(:,20,:) = mat(3:end-cut_off+2,20,:);
    mat2(:,15,:) = mat(3:end-cut_off+2,15,:);
    mat2(:,21,:) = mat(3:end-cut_off+2,21,:);
    mat2(:,14,:) = mat(4:end-cut_off+3,14,:);
    mat2(:,22,:) = mat(4:end-cut_off+3,22,:);
    mat2(:,13,:) = mat(5:end-cut_off+4,13,:);
    mat2(:,23,:) = mat(5:end-cut_off+4,23,:);
    mat2(:,12,:) = mat(5:end-cut_off+4,12,:);
    mat2(:,24,:) = mat(5:end-cut_off+4,24,:);
    mat2(:,11,:) = mat(6:end-cut_off+5,11,:);
    mat2(:,25,:) = mat(6:end-cut_off+5,25,:);
    mat2(:,10,:) = mat(7:end-cut_off+6,10,:);
    mat2(:,26,:) = mat(7:end-cut_off+6,26,:);
    mat2(:,9,:) = mat(8:end-cut_off+7,9,:);
    mat2(:,27,:) = mat(8:end-cut_off+7,27,:);
    mat2(:,8,:) = mat(9:end-cut_off+8,8,:);
    mat2(:,28,:) = mat(9:end-cut_off+8,28,:);
    mat2(:,7,:) = mat(9:end-cut_off+8,7,:);
    mat2(:,29,:) = mat(9:end-cut_off+8,29,:);
    mat2(:,6,:) = mat(10:end-cut_off+9,6,:);
    mat2(:,30,:) = mat(10:end-cut_off+9,30,:);
    mat2(:,5,:) = mat(10:end-cut_off+9,5,:);
    mat2(:,31,:) = mat(10:end-cut_off+9,31,:);
    mat2(:,4,:) = mat(11:end-cut_off+10,4,:);
    mat2(:,32,:) = mat(11:end-cut_off+10,32,:);
    mat2(:,3,:) = mat(11:end-cut_off+10,3,:);
    mat2(:,33,:) = mat(11:end-cut_off+10,33,:);
    mat2(:,2,:) = mat(12:end-cut_off+11,2,:);
    mat2(:,34,:) = mat(12:end-cut_off+11,34,:);
    mat2(:,1,:) = mat(12:end-cut_off+11,1,:);
    mat2(:,35,:) = mat(12:end-cut_off+11,35,:);
end
end

```

```

Mscan = squeeze(mat2(220:330, 7, 10:210));
Mscan_diff = diff(Mscan,[],2);
rawimg = Mscan_diff;
fltr4img = [1 1 1 2 3; 1 1 3 4 2; 1 3 5 3 1; 2 4 3 1 1; 3 2 1 1 1];
fltr4img = fltr4img / sum(fltr4img(:));
imgfltrd = filter2( fltr4img , rawimg );
current_off = 100;
[accum, axis_rho, axis_theta, lineprm, lineseg] = ...
Hough_Grd(imgfltrd(1:76,current_off:163), 800, 0.60);
lineseg(:,1) = lineseg(:,1)+current_off-1;
lineseg(:,2) = lineseg(:,2)+current_off-1;
theta_min = 35;
theta_max = 55;
for i = 1:length(lineseg(:,1))
    theta_line = atand(abs((lineseg(i,3)-
        lineseg(i,4))/(lineseg(i,2)-lineseg(i,1))));
    if (theta_line < theta_min) || (theta_line > theta_max)
        lineseg(i,:) = zeros(4,1);
    end
end
figure(3); imagesc(rawimg); colormap('gray'); axis image;
DrawLines_2Ends(lineseg);
title('Raw Image with Line Segments Detected');

% Process and save all lines
if (1)
    ext = '.png';
    path = 'C:\Documents and Settings\Anthony\My Documents\Thesis\ULA-
OP modes\Acq_Anthony18Jul12\Line_Detect\9.5kA-b3\';
for i = 1:n_lines
    Mscan = squeeze(mat2(230:310, i, 50:190));
    Mscan_diff = diff(Mscan,[],2);
    rawimg = Mscan_diff;
    fltr4img = [1 1 1 2 3; 1 1 3 4 2; 1 3 5 3 1; 2 4 3 1 1; 3 2 1 1 1];
    fltr4img = fltr4img / sum(fltr4img(:));
    imgfltrd = filter2( fltr4img , rawimg );
    current_off = 60;
    [accum, axis_rho, axis_theta, lineprm, lineseg] = ...
        Hough_Grd(imgfltrd(1:66,current_off:123), 800, 0.60);
    lineseg(:,1) = lineseg(:,1)+current_off-1;
    lineseg(:,2) = lineseg(:,2)+current_off-1;
    theta_min = 35;
    theta_max = 55;
    for k = 1:length(lineseg(:,1))
        theta_line = atand(abs((lineseg(k,3)-
            lineseg(k,4))/(lineseg(k,2)-lineseg(k,1))));
        if (theta_line < theta_min) || (theta_line > theta_max)
            lineseg(k,:) = zeros(4,1);
        end
    end
end

figure(1); imagesc(axis_theta*(180/pi), axis_rho, accum); axis xy;
xlabel('Theta (degree)'); ylabel('Phi (pixels)');
title('Accumulation Array from Hough Transform');
figure(3); imagesc(imgfltrd); colormap('gray');

```



```

DrawLines_2Ends(lineseg);
title('M-scan with Highlighted Line','FontSize', 18);
xlabel('Time (ms)','FontSize', 18), ylabel('Time of Flight
      (ns)','FontSize', 18),
oldxlabels=get(gca,'xtick');
newxlabels=round(oldxlabels*2.333);
set(gca,'xticklabel',newxlabels);
oldylabels=get(gca,'ytick');
newylabels=oldylabels*20;
set(gca,'yticklabel',newylabels);
string = sprintf('%d', i);
file_name = ['line', string];
saveas(gcf, [path, file_name, ext], 'png');
end
end

```

## VITA AUCTORIS

NAME: Anthony Lui

PLACE OF BIRTH: Windsor, Ontario

YEAR OF BIRTH: 1988

EDUCATION: Vincent Massey Secondary School, Windsor, Ontario  
2002-2006

University of Windsor, Windsor, Ontario  
2006-2010 B.A.Sc.

University of Windsor, Windsor, Ontario  
2010-2012 M.A.Sc.